UTRECHT UNIVERSITY

MASTER THESIS

INORGANIC CHEMISTRY & CATALYSIS

Catalyst development for the catalytic conversion of ethanol to 1,3-butadiene

Author:
Ewout B.J. Sirks

Supervisors:
Dr. Sang-Ho Chung
Dr. Pieter C.A. Bruijnincx

A thesis submitted in partial fulfillment for the degree of Master of Science

May 7, 2016

This research has been performed within the framework of the CatchBio program. The author gratefully acknowledges the support of the Smart Mix Program of the Netherlands Ministry of Economic Affairs and the Netherlands Ministry of Education, Culture and Science and NWO for funding of the NMR infrastructure (Middelgroot program, grant number 700.58.102).

The cover page has been acquired from http://greenenterprise.ca/GEM/.

"And, when you want something, all the universe conspires in helping you to achieve it."

- Paulo Coelho, *The Alchemist*

Abstract

Butadiene is a compound mainly used in polymer chemistry, which is currently obtained as a side product in naphtha steam cracking. Due to the recent industrial feedstock shift towards shale gas, butadiene supply is limited. Therefore finding a sustainable, on-purpose alternative for butadiene production is desired. The Lebedev process, where (bio)ethanol is converted in butadiene, is a promising alternative due to the wide availability of bioethanol produced in a sustainable manner. It is believed that ethanol is first dehydrogenated towards acetaldehyde. A subsequent aldol condensation and dehydration step yield crotonaldehyde, an α-β unsaturated aldehyde. Selective hydrogenation to crotyl alcohol is desired and a subsequent dehydration step yields butadiene. Previous work has shown that an overall well performing catalyst is a mixture of SiO_2 and MgO, where a wet-kneaded catalyst produces more butadiene than co-precipitated or physically mixed catalysts. It is believed that magnesium silicates formed during wet-kneading are beneficial for ethanol conversion.
Being an unconventional synthesis procedure, the wet-kneading parameters were optimised. Particularly following the wet-kneading time proved insightful, as the formation of magnesium silicates could be followed. TEM images showed the occurance of severe morphological changes during wet-kneading, caused by cross-deposition of dissolved species on both SiO_2 and MgO surfaces. This was verified by recording EDX maps of the wet-kneaded catalysts with different wet-kneading time. XRD patterns of these catalysts showed a decrease of crystalline phases, but the particle size was unaffected. FT-IR spectroscopy showed that during wet-kneading, magnesium silicates are formed which seem to correlate to the ethanol conversion. However, the exact composition of these magnesium silicates could not be quantified by FT-IR. The wet-kneading time varied catalysts were therefore analysed by ^{1}H-^{29}Si cross polarised - magic angle spinning NMR to determine the phase distribution of these magnesium silicate species. The hydrous layered magnesium silicates (e.g. talc, stevensite, lizardite) were suggested to be beneficial for butadiene formation and the hydrous amorphous magnesium silicates for ethylene formation, but it has to be noted that both SiO_2 and MgO contribute on its own to the reaction as well.
Secondly, previous work showed that the addition of Cu to the wet-kneaded catalyst increased the butadiene selectivity, but deactivation was observed. Therefore the wet-kneaded catalyst was impregnated with several transition metals to increase the redox properties. Cu and Ag promotion yielded the highest initial activity. Most catalysts showed strong deactivation over time, assumed to arise from severe carbonaceous deposition. The promoted catalysts suffered from more carbonaceous deposition compared to the unpromoted catalyst. Mn promoted SiO_2-MgO showed a moderate increase in butadiene selectivity, but possessed a higher resistivity towards coke formation and thus deactivation.
Looking forward, producing and testing pure or metal promoted layered hydrous magnesium silicates is the next step, as it is known from literature that talc and sepiolite contribute to the Lebedev process. Secondly, further analysis needs to be carried out on the promoted wet-kneaded catalysts to clarify the oxidation state and active sites. Subsequently, varying metal loading and alloying are the next steps in the promoter studies. Finally for potential upscaling experiments, catalyst regeneration has to be studied.

Table of Contents

1 Introduction

Today's society is highly dependent on crude oil. Many household products consist of naphtha derived chemicals: plastic bags are built up from ethylene polymers, cosmetics contain mostly industrially produced chemicals, clothing consists of nylon-6,6 and other polyesters; the list of petrochemically derived products is somewhat infinite. But crude oil is most of all used to keep our cars running; obviously as a fuel, but car tires are derived from crude oil as well. Keeping the future in mind, it would be ideal if alternative production routes for these petrochemicals could be established. Research is nowadays focussing on producing the same petrochemicals in a more sustainable manner by e.g. converting biomass towards bulk chemicals. A good example is the fermentation of sugars towards bioethanol, which accounts for 90 % of the total ethanol production. Fig. 1 depicts the global ethanol production over the past decades, which sharply increased in the new millenium. In recent years, bioethanol production increased even further. In 2011, 105 billion liters of bioethanol was produced globally with an expected annual growth of 3-7%.[2] Although most bioethanol is used as a transportation fuel, it is considered as a promising, renewable building block for various bulk chemicals such as ethylene and acetaldehyde, but also for larger molecules such as 1,3-butadiene.[1]

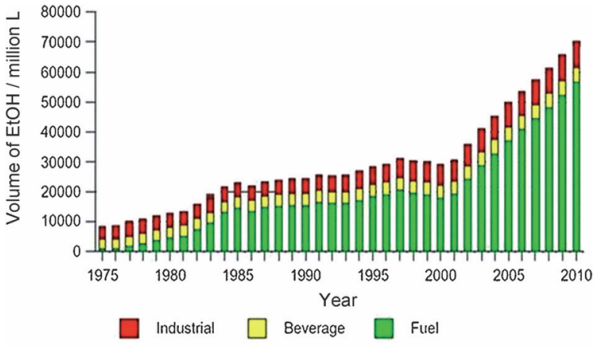

Fig. 1. *Global annual ethanol in the period 1975-2010.*[1]

1,3-Butadiene (or butadiene for short) is an important monomer in polymer industry with a high annual demand (10.5 million tons in 2011[3]), especially for synthetic rubbers. The global butadiene consumption volume is depicted in Fig. 2. Butadiene is mostly converted to poly-butadiene and styrene-butadiene rubbers (BR and SBR). These rubbers are used in a large variety of downstream products, but BR and SBR are mostly used in e.g. car tires, latex rubbers (SB latex) and shoe soles.[4] Nitrile-butadiene rubbers (NBR) and Neoprene (2-chloro-1,3-butadiene) polymers are used in chemical protection gear (e.g. laboratory gloves) because of its high chemical resistance.[4,5] Butadiene is also used for electronic device resins production such as acrylonitrile- butadiene-styrene (ABS) and hexamethylene diamine (HMDA) production, which is a precursor for nylon 6-6.[4]
Currently, butadiene is mainly obtained from naphtha steam cracking as a byproduct of the ethylene production process.[4,6,7] Due to recent trends towards using light feedstock in industry such as shale gas, it is expected that the cracker output consists of a significant lower C_4 fraction as seen in Fig. 3. These shifts resulted in a shortage in C_4 chemicals including butadiene, doubling the butadiene prices compared to 2007.[6] Furthermore, fossil fuels are a limited and finite resource and its reserves are depleting. Therefore, finding an alternative and on-purpose butadiene production process from renewable resources is highly desirable.

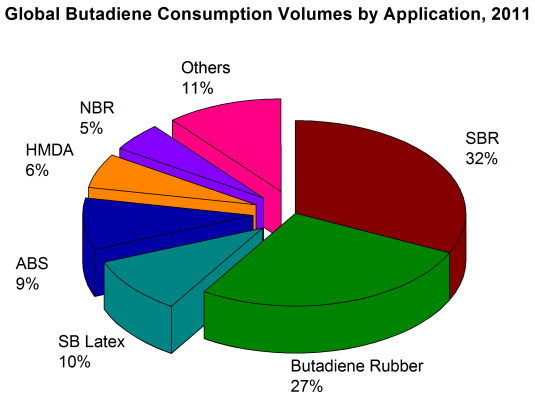

Fig. 2. Global consumption fractions of butadiene in various products. Reproduced from TMR.[3]

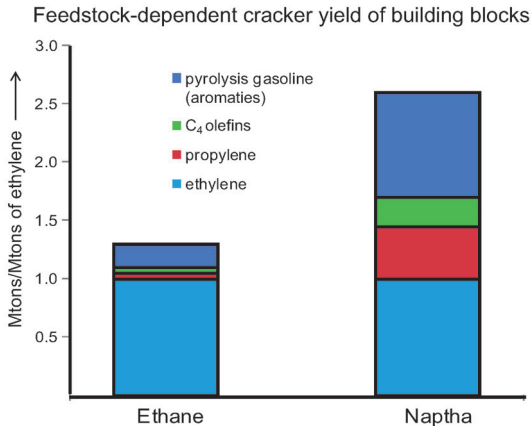

Fig. 3. Cracker output using different feedstocks.[6]

Butadiene can alternatively be produced from different feedstocks such as n-butane, n-butanol and n-butenes,[5] but ethanol as well[8] (Fig. 4). Amongst the potential butadiene precursors, the ethanol-to-butadiene reaction is particularly attractive, since ethanol can be produced in such a sustainable manner.[1] Notably, the synthesis process of butadiene from ethanol was already developed in the beginning of the 20th century. First reports of the ethanol-to-butadiene reaction came from the Russian Empire in 1903, where Ipatiev observed slight butadiene formation (1.5 % yield) when ethanol was flowed over powdered alumina.[9] In 1915, Ostromislensky found that the butadiene yield could be increased to 18% using acetaldehyde as a co-fed reactant. This reaction is often referred to as the two-step, or Ostromislensky process.[10] In 1929, Lebedev patented a direct ethanol-to-butadiene process with a catalyst consisting of a mixture of different oxides, mostly magnesia and silica.[11] This reaction is commonly referred to as the one-step, or Lebedev process. For process simplicity reasons and thus its applicability in industry, the Lebedev process is preferred over the Ostromislensky process. In the 20th century, the Lebedev process was used on large scale in the Soviet Union during the Second World war due to a large availability of grain ethanol. The butadiene rubbers demand was at that time high for military purposes.[12] In the 1960s, butadiene production from steam cracking of fossil fuels was economically preferred over the ethanol-to-butadiene process, with the result that the process lost its competitiveness.[6] However, recent techno-economic analysis shows that the bioethanol-based route is advantageous than the naphtha-based route based on process simplicity and cost reduction, which led to an increased academic interest in the bioethanol-to-butadiene process.[13,14] Furthermore, due to a larger consumption of ethanol and higher investment costs needed in the Ostromislensky process, the Lebedev process is in sustainability point of view preferred.[15] Unfortunately, no catalyst has yet been produced to make the Lebedev process industrially viable and competitive with the naphtha-based route,[1] nowadays further caused by the low price of crude oil.

Catalyst production for the Lebedev process has been studied extensively, using a large variety of supports and promoters.[1,12] To further study on Lebedev's work, SiO_2 and MgO mixtures have been optimised, by e.g. addition of a promoter to influence rate determining steps in the Lebedev process. Pioneering in this work, Natta and Rigamonti showed a Cr promoted SiO_2-MgO mixture to yield 42 % butadiene.[16] Especially Cu[17] and Ag[18] promoters have shown promising enhancement of catalytic performance of SiO_2-MgO mixtures, with butadiene yields reported over 50 %. Other promising Lebedev catalysts and their respective butadiene selectivities are Hf-Zn/SiO_2 (70 %),[19] Ag/ZrBEA (>60 %).[20] Upscaling is the next step for all these materials, to possibly compete against the naphtha-based butadiene production pathway.

Here, the synthesis of active Lebedev catalysts is discussed. A silica-magnesia (SiO_2-MgO) mixture was further optimised. First, a theoretical background and summary of previous work is given, followed by the project aims. The experimental section, results and discussion are then presented to show the work carried out. Finally, a conclusion and outlook are given.

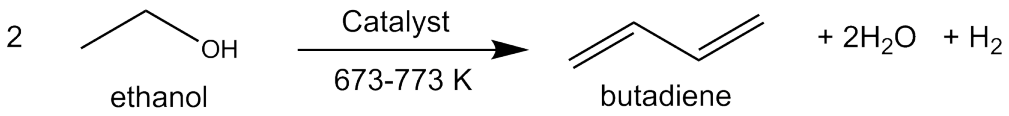

Fig. 4. *Overall reaction of the Lebedev process.*

2 Theoretical background

2.1 Mechanism

Although many studies have proposed the mechanism of the Lebedev process,[21–24] it still has not been confirmed. Fig. 5 shows the commonly accepted mechanism of the one-step ethanol-to-butadiene reaction.

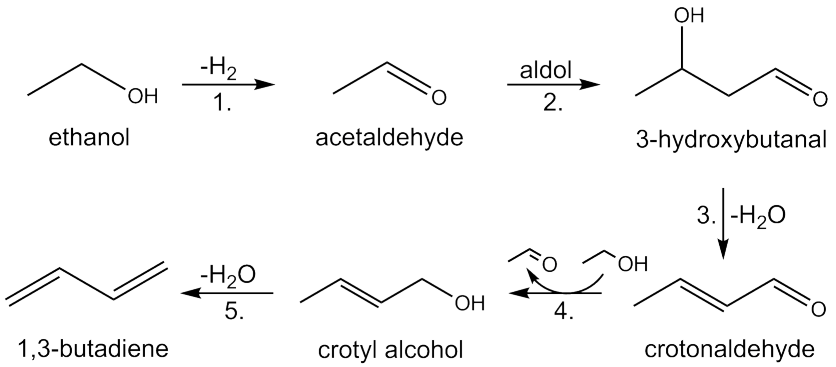

Fig. 5. *Commonly proposed mechanism for the Lebedev process of ethanol into 1,3-butadiene, with each step numbered subsequently.*[25,26]

Many different materials have been tested as catalysts in the Lebedev reaction, but it has been shown that a mixture of SiO_2 and MgO has shown to perform exceptionally well, with a good reproducibility.[1,12,27] According to the proposed mechanism, the Lebedev process requires a multifunctional catalyst, containing redox active sites for the (de)hydrogenation reaction in steps 1 and 4 (e.g. a metal oxide/metal redox couple), basic sites for aldol condensation in step 2 (e.g. supplied by MgO) and acid sites for dehydration for steps 3 and 5 (e.g. supplied by SiO_2).[12,27] The amount of acidic and basic sites is of vital importance for the Lebedev reaction. To illustrate, a large amount of acidic sites and strong basic sites present on the catalytic surface causes mainly dehydration of ethanol, with the main side products being ethylene and diethyl ether. A low amount of acidic sites however, prevents the crucial dehydration reactions in steps 3 and 5, limiting the butadiene yield. This shows the necessity of a fine balance between acidity and basicity, where it was postulated that the presence of an intermediate amount of acidic sites and a low amount of strong basic sites give the best performing catalyst.[28] Notably, the SiO_2-MgO catalyst does show activity, without the requirement of an additional redox-active species. Steps 1 and 4 in Fig. 5 can namely proceed through the Meerwein-Ponndorf-Verley (MPV) reduction, which can be catalysed by MgO.[29] The MPV reduction ocurring in the Lebedev process takes place in step 4 of Fig. 5, where crotonaldehyde is reduced to yield crotyl alcohol and the ethanol is oxidised to acetaldehyde. The catalyst assists in hydrogen transfer between the aldehyde and the alcohol.
When the feedstock crosses the catalyst bed, the ethanol needs to be brought in contact with a redox- or MPV-active site first in order for the Lebedev process to continue. The feedstock can however coordinate to an acidic site as well, resulting in dehydration of ethanol, yielding e.g. ethylene and diethyl ether. It is therefore believed that the dehydrogenation reaction in step 1 is the rate determining step,[30] although thermodynamic calculations indicate that aldol con-

densation is unfavourable due to a decrease in entropy.[12,25] To further circumvent unwanted ethylene formation, a promoter can be added to facilitate (de)hydrogenation properties of the catalyst. It has to be noted that the hydrogenation of crotonaldehyde to crotyl alcohol over a metal promoter is considered as a challenging step, as the selective hydrogenation of the aldehyde group is needed to produce butadiene, instead of the C=C bond. Thermodynamics actually prefer C=C hydrogenation over C=O hydrogenation by approximately 35 kJ mol^{-1}.[31] Secondly, due to kinetics the reactivity of the C=C bond is higher than the C=O.[31,32] Apparently for SiO_2-MgO catalysts, MPV reduction is favoured over selective hydrogenation, as butadiene is the main observed product. Nonetheless, a promoter could resolve this matter to increase the dehydrogenation and selective hydrogenation properties of the catalyst. Transition metals are often used as such promoters, but their activity changes when the d band is filled, resulting in a difference in electronic structure. Promoters as Pd or Pt have too high hydrogenating properties, which will rather hydrogenate the C=C bond,[32–34,34,35] most likely yielding butyraldehyde, 1-butanol and n-butane as a main products in the Lebedev reaction. Therefore, promoters with a preference towards selective C=O hydrogenation, such as Cu,[17] Ag[18] or Zn[36,37] could be introduced to the catalyst to selectively hydrogenate crotonaldehyde to crotyl alcohol.
Promoter effects on the competitive and selective aldehyde hydrogenation of α-β- unsaturated aldehydes as crotonaldehyde,[31,38] but also cinnamaldehyde could be implemented in the Lebedev process, since the same selectivity is desired (Fig. 6). Cinnamaldehyde can be converted to cinnamyl alcohol and to hydrocinnamaldehyde by a variety of transition metal promoters. For example, Mo[39] and Co[40,41] gave yield to cinnamyl alcohol with high selectivities.

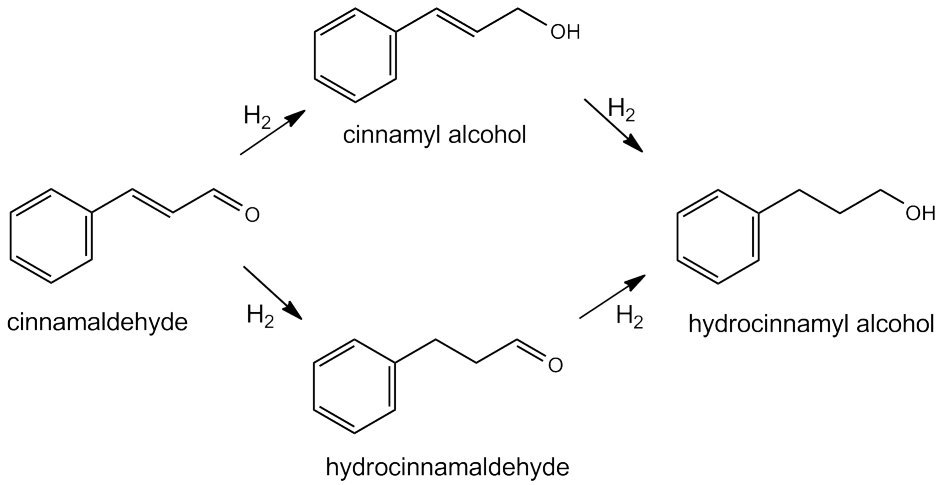

Fig. 6. *Hydrogenation pathways of cinnamaldehyde.*[40]

2.2 Previous work

The Lebedev process has been studied extensively. Not only for being an attractive alternative for the petrochemical industry, but academia prefer the Lebedev process as well. Due to the single reactant used, it is more facile to investigate the mechanism, kinetics and catalytic activity.[21–24] As previously stated, a mixture of SiO_2 and MgO is a typical Lebedev catalyst.[1,12] The individual components or a physical mixture do not show activity in the Lebedev process, where previous work in our group showed that SiO_2 is inert and MgO produces slight amounts (<3 %) of ethylene and acetaldehyde under Lebedev conditions. Further experiments showed that SiO_2-MgO mixtures are sensitive to different chemical synthesis techniques. Fig. 7 shows that wet-kneaded materials have an increased activity, compared to a co-precipitated compound or a physical mixture of the catalyst precursors, where it has been found that during wet-kneading, magnesium silicates essential for the catalytic activity are formed.[17]

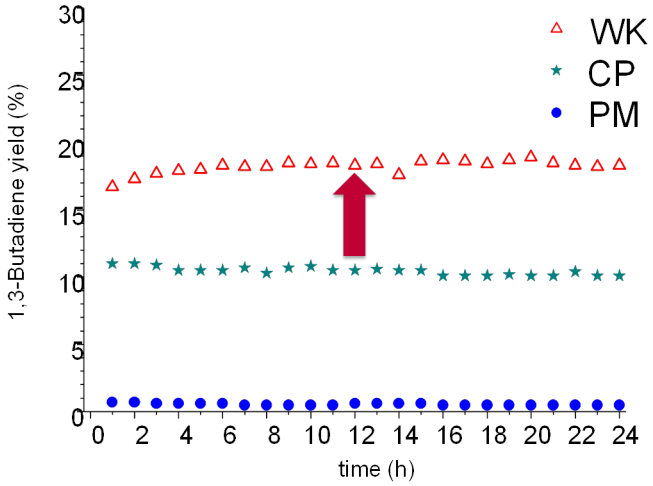

Fig. 7. *Butadiene yield for wet-kneaded (WK), co-precipitated (CP) and physically mixed (PM) SiO_2-MgO catalysts.*[17]

The term "wet-kneading" was first introduced by Natta et *al.*[16] and further used as a Lebedev catalyst synthesis method by Kvisle et *al.*,[42] with its definition nowadays proposed as a process where two or more solid precursors are suspended and stirred (mechanically or magnetically) thoroughly in a liquid medium.[43] In this work, Stöber SiO_2 and $Mg(OH)_2$ are mixed in water and afterwards calcined. Looking at the selectivity difference in Fig. 7, it is evident that the catalytically active species are formed during wet-kneading.
In wet-kneading, the pH varies significantly. This is explained by initially a slight dissolution of $Mg(OH)_2$, yielding Mg^{2+} and OH^- ions,[44] yielding an alkaline medium in which wet-kneading is carried out. The obtained increase in pH causes a dissolution of SiO_2, yielding $[SiO_2(OH)_2]^{2-}$ species.[45] Due to the opposite surface charges of $Mg(OH)_2$ and SiO_2 caused by the difference in isoelectric point (pH >12 and pH = 2, respectively), it is proposed that the Mg^{2+} cations deposit on the anionic SiO_2 surface, and the $[SiO_2(OH)_2]^{2-}$ anions on the cationic $Mg(OH)_2$ surface. Due to the redeposition of the dissolved species, the pH decreases again. STEM-EDX

analysis by Chung et *al.* confirmed the cross-deposition of dissolved species on both SiO_2 and $Mg(OH)_2$ surfaces,[43] meaning that both SiO_2 and $Mg(OH)_2$ dissolve and redeposit in small amounts when wet-kneaded. Characterisation of these newly formed species was initially carried out with FT-IR spectroscopy, which showed the presence of the hydroxyl groups on the catalyst surface (Fig. 8). Compared to pure SiO_2 and MgO, the wet-kneaded catalyst showed a new signal around 3670 cm^{-1}, which must originate from a new species formed during wet-kneading. This was assigned to the Mg-OH-Si stretching vibration, typically found in magnesium silicates.[28] The intensity of the peak of the magnesium silicates found in IR spectroscopy seemed to correlate to the ethanol conversion. The signal however consists of different types of magnesium silicates, so it is difficult to determine which species is beneficial for butadiene selectivity. To illustrate, antigorite, $Mg_3Si_2O_5(OH)_4$, shows a sharp peak at 3670 cm^{-1},[46] but talc, $Mg_3Si_4O_{10}(OH)_2$, shows a peak at 3674 cm^{-1}.[47] Therefore, the amount of these magnesium silicates cannot be quantified using FT-IR.

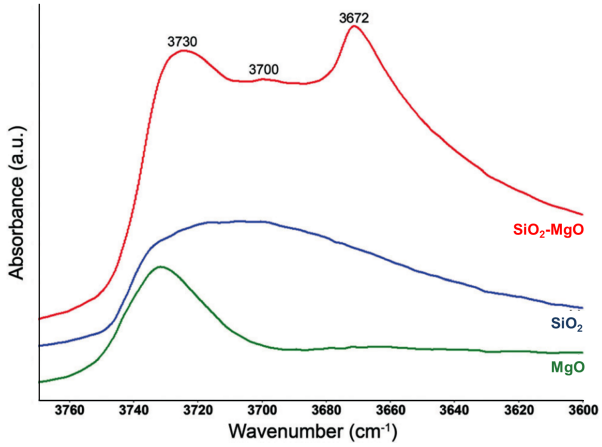

Fig. 8. *FT-IR spectra of MgO in green, SiO_2 in blue and the wet-kneaded SiO_2-MgO catalyst in red. The spectra are offset for clarity.*[28]

Magnesium silicates are known to contribute to the catalytic activity in the Lebedev process. For example, Zn promoted talc[37] and Ag promoted sepiolite[48,49] show selectivity towards butadiene. Unpublished work from our group showed that pure talc and MgO are not active individually, but a mixture of MgO and commercially available talc yields an active species, albeit highly selective towards butanol.

Furthermore, it has been shown that decreasing the precursor particle size yielded a more active catalyst. This was attributed to a higher intimacy of the components and a difference in acid-base properties.[17] Unpublished work from our group showed that decreasing the magnesium hydroxide particle size especially influenced the butadiene yield (Fig. 9). The MgO precursor was prepared by dropwise addition of 1 M ammonia to a magnesium nitrate solution, which was aged over night. This resulted in particles with dimensions of approximately 200 by 40 nm. The smaller MgO precursor (”nano”MgO or nMgO) was synthesised by dropwise addition of NaOH to magnesium nitrate and aged for 1 h.[50] The dimensions of these particles were approximately 100 by 20 nm.

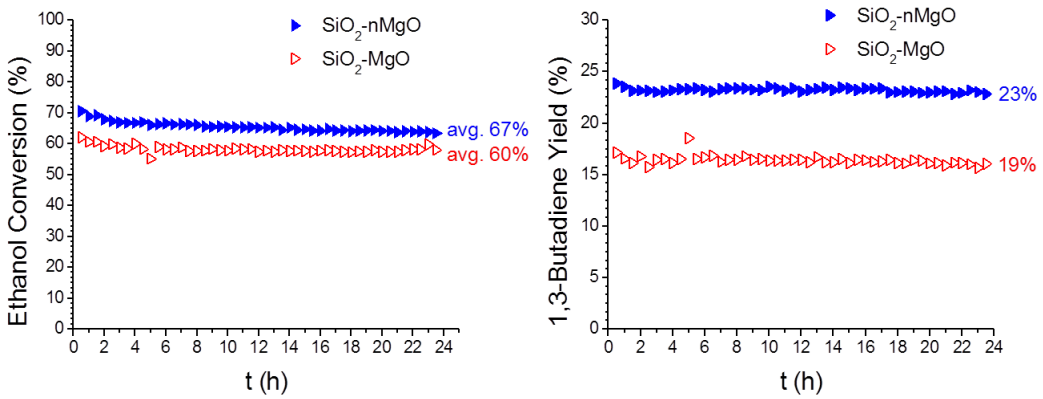

Fig. 9. *Ethanol conversion (left) and butadiene yield (right) for the wet-kneaded SiO_2-MgO catalyst in red and the wet-kneaded SiO_2-nMgO catalyst in blue.*

Using this nMgO, it has been shown that a Si/Mg molar ratio of 1 yields the best performing catalyst, with the correct amount of acidic and basic sites formed during wet-kneading. However, the optimal ratio is still debated, as other researchers found lower Si/Mg ratios to be more beneficial.[18,51–53] To emphasise, these authors used different SiO_2 or $MgO_/Mg(OH)_2$ sources than used in previous work in our group.[28,43] The IR spectra of nMgO, SiO_2 and wet-kneaded SiO_2-nMgO are given in Fig. 10. Compared to Fig. 8, the intensities of the nMgO and the typical magnesium silicate band are slightly lower. This indicates that the total amount of magnesium silicates between the two catalysts differs. Beneficial magnesium silicates are thought to be more abundant in the SiO_2-nMgO catalyst, giving rise to an increased butadiene yield.

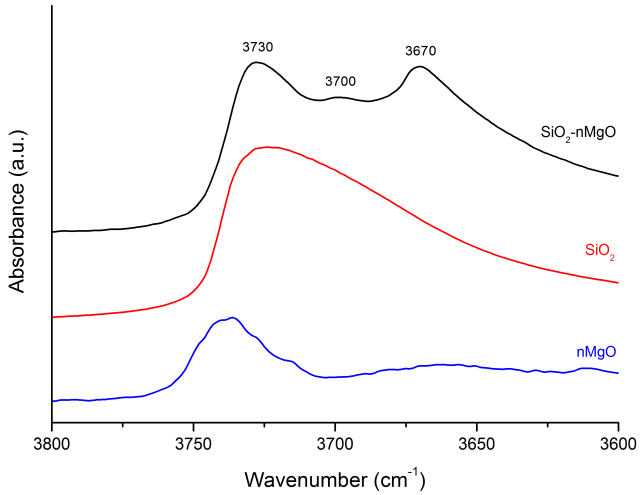

Fig. 10. *FT-IR spectra of nMgO (blue), SiO_2 (red) and wet-kneaded SiO_2-nMgO in black. The spectra are offset for clarity.*[43]

3 Aim

Wet-kneading proves to be a good synthesis method for SiO_2-MgO catalysts, where wet-kneaded catalysts show higher catalytic activity compared to other synthesis methods. However, wet-kneading is an unfamiliar synthesis method for preparing catalysts. It is therefore attempted to elucidate the process for a better understanding. The wet-kneading parameters will be optimised in terms of precursor particle size, amount of water used for wet-kneading and wet-kneading time. Particularly varying the wet-kneading time proved insightful, as it was possible to follow the magnesium silicate formation. Furthermore, the addition of a buffer was carried out to see the effect of pH influences during wet-kneading.
As previously stated, FT-IR yields insufficient information about the exact composition of magnesium silicates. Therefore, ^{1}H-^{29}Si cross polarised - magic angle spinning (CP-MAS) NMR was carried out for the catalysts with varied wet-kneading time, to determine the different magnesium silicate phases formed during wet-kneading.
Furthermore, previous work attempted to improve the redox properties of the catalyst using Cu promoted wet-kneaded SiO_2-MgO catalysts to improve the catalysts (de)hydrogenation properties.[17] Although the activity and selectivity towards butadiene increased, the catalyst deactivated rapidly. This was ascribed due to the effect of the formation of carbonaceous compounds. Therefore, the catalyst will be loaded with a variety of transition metals to possibly yield a better performing catalyst with higher stability. For example the addition of Zn, Zr and Ag to a SiO_2-MgO catalyst have been studied to large extents in the Lebedev process and appear to be beneficial for butadiene formation.[1,12,18,54,55]

4 Wet-kneading optimisation

4.1 Introduction

Introduced by Natta and Rigamonti[16] and further used by Kvisle et *al.*,[42] wet-kneading proves to be a new synthesis technique capable of influencing the catalyst phase. It is clear from Chapter 2.2 that the catalyst is chemically modified during wet-kneading. Although wet-kneaded catalysts showed improved catalytic activity than catalysts prepared by other methods,[17] little is known about wet-kneading itself. Therefore, the wet-kneading parameters will be varied to obtain insights about wet-kneading itself; and optimised by changing the amount of water present, wet-kneading time and precursors.

4.2 Experimental procedure

4.2.1 Materials

$Mg(NO_3)_2{\cdot}6\,H_2O$ (99+%, Acros), $MgSO_4{\cdot}7\,H_2O$ (Aldrich), NaOH (Merck), $Si(OC_2H_5)_4$ (TEOS, 98%, Aldrich), NH_4OH (28-30%, Merck), C_2H_5OH (100%, Interchema) and HNO_3 (65%, Merck) were used for the preparation of catalyst precursors. NH_4NO_3 (Aldrich) was used as a buffer during wet-kneading for pH influence experiments. Commercially available Aerosil 300 (Evonik) and 380 (Degussa) were used in wet-kneading as a SiO_2 source with smaller dimensions.

4.2.2 Catalyst preparation

For catalyst production, nano-sized magnesium hydroxide ($nMg(OH)_2$) and silica were used as precursors. To produce $nMg(OH)_2$, 0.4 M NaOH (Merck) was drop wise added to 250 ml 0.2 M $Mg(NO_3)_2$ solution, while stirring at 600 rpm. When the pH reached 12, the solution was stirred for 1 h. After centrifugation, the obtained precipitate was redispersed in water as a washing step. Finally this dispersion was centrifuged and dried at 393 K. After grinding a white powder was obtained.
SiO_2 was synthesised via a Stöber analogue. 17.3 g TEOS was added to a mixture of 230 ml ethanol and 11.25 g ammonia preheated to 308 K. After 15 h, the mixture was neutralised with 8.7 ml nitric acid. After rotary evaporation for 1.5 h, a white powder was obtained.
For the reference catalyst, wet-kneading was performed with the individual components. 1.029 g $nMg(OH)_2$ and 1.060 g SiO_2 (corresponding to a Si/Mg molar ratio of 1) were ground together for 10 min using a mortar and pestle. The mixture was then kneaded in 200 ml water at 600 rpm for 4 h. After centrifugation, the product was first dried at 393 K and subsequently calcined for 5 h at 773 K. The calcined material was sieved to a particle size between 90 and 425 μm to yield the catalyst.
Variations in wet-kneading time and the amount of water used for wet-kneading were applied to the wet-kneading process. Furthermore, precursors were varied by using commercially available chemicals (Aerosil 300 and 380) or changing the magnesium source ($MgSO_4{\cdot}7\,H_2O$ instead of $Mg(NO_3)_2{\cdot}6\,H_2O$). The effect of NH_4NO_3 addition during wet-kneading was tested as well.

4.2.3 Catalyst testing

0.12 g quartz wool and 0.2 g catalyst (sieved to 90-425 μm) were put in a quartz glass reactor. The reactor was heated to 698 K and left for 1 h as catalyst pretreatment. The desired amount of ethanol was introduced to the reactor using a Bronkhorst CEM system, which consists of a liquid flow controller to control the amount of ethanol, a gas flow controller for the nitrogen carrier gas and a mixing chamber kept at 303 K. The gaseous mixture consisting of 2 ml min^{-1} ethanol and 98 ml min^{-1} N_2 was flowed through the reactor. The reaction mixture was analysed by GC-FID (gas chromatography with flame ionization detector) using a CP poraplot Q-HT column. Quantification of the main components (ethanol, ethylene, acetaldehyde, butadiene, and diethyl ether) was based on calibration curves obtained by feeding known amounts of these compounds directly to the GC.

4.2.4 Characterisation

Transmission electron microscopy (TEM) images of the various samples were obtained on a Tecnai 12 apparatus, operated at 120 keV. The catalyst particles were sonicated in ethanol and deposited on a carbon coated Cu TEM grid prior to analysis. EDX maps were acquired on a FEI Talos F200X microscope operated at 200 keV, equipped with a superX EDX detector. Bruker Esprit software was used to record the data. iTEM software was used to calculate particle sizes. X-ray powder diffraction (XRD) patterns were obtained by a Bruker-AXS D2 Phaser powder X-ray diffractometer using Co K$\alpha_{1,2}$ with = 1.79026 Å, operated at 30 kV. Measurements were carried out in the range 10-100 2θ degrees using a step size of 0.15 2θ degrees and a scan speed of 0.5 s.
NH_3-TPD measurements were performed on a Micromeritics ASAP2920 apparatus. Typically, 0.2 g catalyst was placed in a quartz reactor. The samples were dried in the apparatus in a helium flow by heating with a temperature ramp of 5 K min^{-1} to a maximum temperature of 873 K. Subsequently, the sample was cooled to 373 K. At this point, NH_3 pulses of 25.31 cm^3 min^{-1} were applied. The sample was then heated to 873 K with a ramp of 5 K min^{-1} to induce desorption of NH_3. The temperature was kept constant once it reached 873 K for 30 min.
Fourier transform infrared spectroscopy (FT-IR) measurements were taken with 25 scans per spectrum on a Perkin Elmer System 2000 with a DTGS detector and a resolution of 4 cm^{-1}. Approximately 17 mg of the catalyst were pressed into a pellet and placed into the infrared measurement cell. The catalyst was dried in the cell under vacuum with a temperature ramp of 5 K min^{-1} reaching the desired temperature of 823 K ; FT-IR spectra were taken every 25 K in the temperature range 323-823 K. Once 823 K was reached, this temperature was kept constant for 30 min; spectra were taken at 5, 10 and 30 min after reaching the maximum temperature.
For catalysts with wet-kneading time , solid-state nuclear magnetic resonance (NMR) experiments were recorded on a Bruker spectrometer operating at a ^{1}H Larmor frequency of 500 MHz, equipped with a 3.2 mm magic angle spinning (MAS) probe, using a 12 kHz MAS frequency and at a temperature of 298 K. After a 94 kHz ^{1}H excitation pulse, Hartmann-Hahn ^{1}H-^{29}Si cross-polarisation (CP) was achieved using a 58 kHz ^{1}H field with a 70-100% ramp, a 71 kHz ^{29}Si field and a contact time of 8 ms. During acquisition 31 kHz SPINAL64, ^{1}H decoupling was applied and a 4 s inter-scan delay was used. Spectra were processed using a 50 Hz line broadening and referenced to tetramethylsilane (TMS). The spectra were deconvoluted using

MestReNova software (ver. 10.0.2), assuming a Gaussian distribution for each deconvoluted signal, which yielded the absolute peak area of the deconvoluted signals.[43]

4.3 Results and discussion

4.3.1 Wet-kneading precursor variation

As mentioned before, decreasing the precursor particle sizes had a positive influence on the catalytic performance of the wet-kneaded catalyst, due to a higher degree of intimacy between the precursors and a difference in acidity and basicity. It was therefore attempted to further decrease these particle sizes. First, high surface area SiO_2 (Aerosil 300 and 380 $m^2\ g^{-1}$) were tested as a smaller silica source than the synthesised Stöber SiO_2 (139 $m^2\ g^{-1}$).[17] The TEM images of Aerosil 380 and the wet-kneaded Aerosil 380-nMgO catalyst are given in Fig 12c and 13b respectively. Aerosil 380 looks similar to data given by the supplier and comparable to TEM images of Aerosil 300 (Appendix 1 and 2).[56] The Aerosil particles appear to be smaller compared to the Stöber SiO_2 spheres (Fig 12a). The catalytic data shown in Fig. 11 depicts that for wet-kneaded Aerosil-nMgO catalysts the butadiene yield decreased significantly compared to the wet-kneaded Stöber SiO_2-nMgO catalyst, but the catalytic performance differs between the used Aerosils as well. It was therefore concluded that the precursor synthesis method influenced wet-kneading as well, as both Aerosils are produced by different suppliers. It was assumed that Stöber SiO_2 is a more beneficial precursor due to its monodispersity.

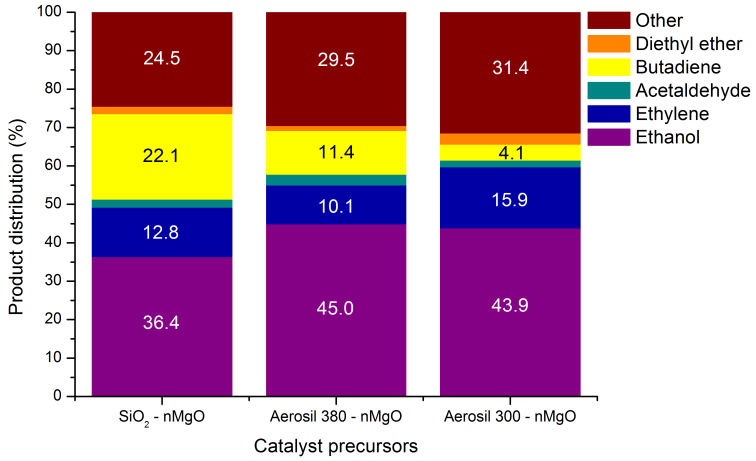

Fig. 11. *Product distribution of the wet-kneaded SiO_2-nMgO and Aerosil-nMgO catalysts. The catalytic data were obtained after 4 h on stream.*

Decreasing the particle size of MgO was attempted by using $MgSO_4{\cdot}7\,H_2O$ rather than $Mg(NO_3)_2 \cdot 6\,H_2O$. Literature stated that in this fashion, needle-like MgO particles are obtained with a smaller surface area (from here referred to as "sMgO"), rather than the platelet-like MgO particles obtained from $nMg(OH)_2$ as a precursor.[57,58]

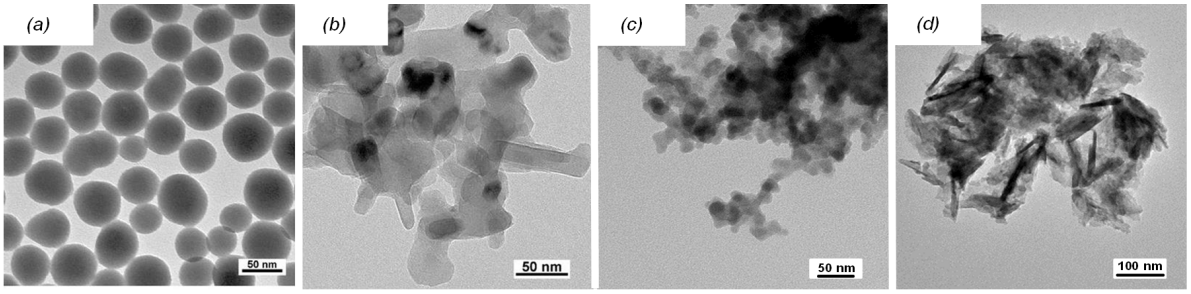

Fig. 12. *TEM images of (a) Stöber SiO_2, (b) nMgO, (c) Aerosil 380 and (d) sMgO.*

The sMgO particles indeed yield a needle like structure (Fig. 12c), compared to nMgO (Fig. 12b). To emphasise, all Mg precursors have smooth surfaces before wet-kneading. In Fig. 13 however, morphological changes were observed after wet-kneading. This will be explained in detail in Chapter 4.3.3. Concomitantly, the needle-like MgO domains are preserved after wet-kneading (Fig. 13c). The average particle size of sMgO needles is 100 by 20 nm, which is the same for the nMgO platelets determined in unpublished work from our group (see Chapter 2.2). From these 2D TEM images, it cannot be concluded if the orientation and/or the third dimension of the sMgO needles is similar as for the nMgO platelets. However, the dimensions of sMgO seem to be smaller than nMgO. For example 3D tomography studies could prove this statement.

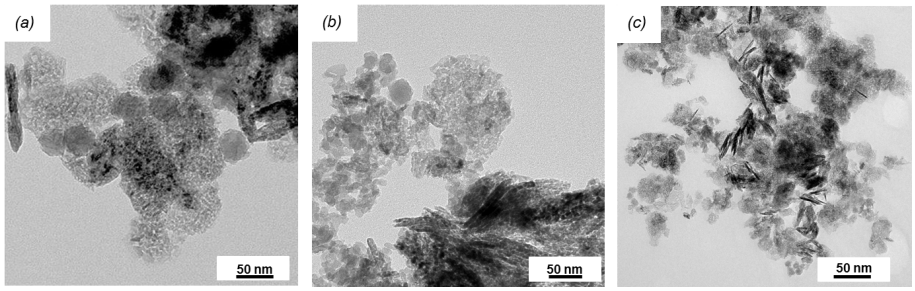

Fig. 13. *TEM images of the wet-kneaded (a) SiO_2-nMgO (b) Aerosil 380-nMgO and (c) SiO_2-sMgO catalysts.*

IR spectroscopy depicted in Fig. 14 showed an increased amount of magnesium silicates, compared to the standard wet-kneaded catalyst. This led to the assumption that a more active catalyst was synthesised. Unfortunately due to technical malfunctions, the catalytic data could not be quantitatively obtained. However, if the initial data obtained were linearly extrapolated, it could be seen that the wet-kneaded SiO_2-sMgO catalyst showed an increased ethanol conversion, but showed higher deactivation. The amount of butadiene and ethylene remained initally the same, but decreased faster over time as well, compared to the SiO_2-nMgO catalyst. Inductively Coupled Plasma - Optical Emission Spectrometry (ICP-OES) analysis confirmed the presence of residual sulphur in the catalyst, which could be the cause of the faster deactivation.
Other methods for further decreasing the MgO particle size without possible poisoning due to counterions could be done by means of a microwave reactor, which can yield nanoparticles with dimensions of approximately 11 nm.[59] Drying a mixture of dissolved magnesium nitrate,

glycine and urea is stated to yield MgO nanoparticles with dimensions between 3-7 nm,[60] but this result could not be reproduced.

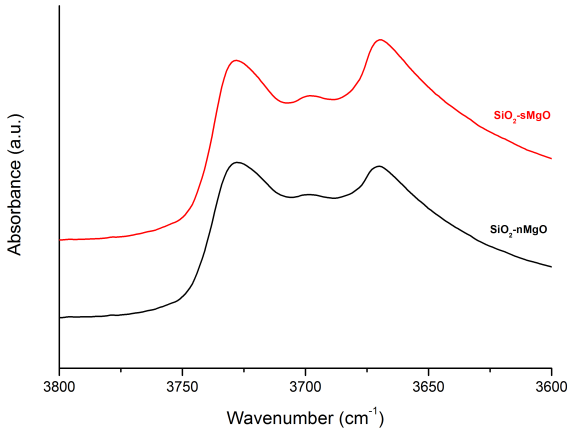

Fig. 14. *IR spectra of the wet-kneaded SiO_2-sMgO catalyst in red and the wet-kneaded SiO_2-nMgO catalyst in black. The spectra are offset, for clarity.*

4.3.2 Wet-kneading volume variation

The amount of water used for wet-kneading was varied, changing the precursor-to-solvent ratio. It was believed that this possibly influenced the amount of dissolved species and thus the formation of magnesium silicates.

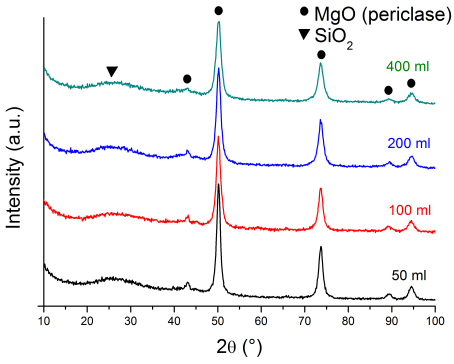

Fig. 15. *XRD patterns of the SiO_2-nMgO catalysts with different wet-kneading volume.*

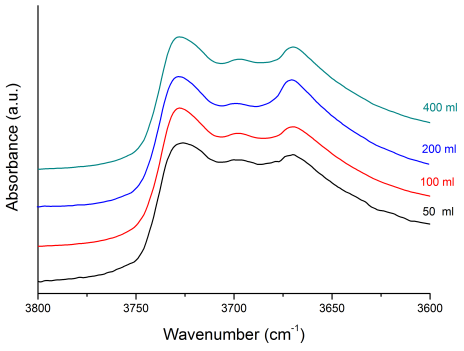

Fig. 16. *FT-IR spectra of the SiO_2-nMgO catalysts with different wet-kneading volume. The spectra are offset, for clarity.*

Fig. 15 shows the XRD patterns of the SiO_2-nMgO catalysts with different wet-kneading volume. The broad band around $2\theta = 25\ ^\circ$ belongs to SiO_2, where the rest of the marked signals belong to the periclase phase of MgO. Fig. 16 shows the IR spectra of these catalysts. For the catalyst wet-kneaded in 50 ml of water, the XRD patterns show a higher intensity of the periclase signals. This could be caused by less dissolved species and thus less cross-deposited species during wet-kneading, causing a lower amount of magnesium silicates to be formed. In Fig. 16, the typical magnesium silicate vibration around 3670 cm^{-1} seems weaker in intensity for this catalyst as well, compared to the other spectra. For the other catalysts, most magnesium silicates seem to have been formed for a wet-kneading volume of 200 ml according to the IR spectrum. The decrease in magnesium silicates for a wet-kneading volume of 400 ml was explained by less intimacy between the dissolved and solid species. Concluding, the variation of wet-kneading volume does not influence the cross-deposition beneficially.

Catalytic testing results of the catalysts with different wet-kneaded volume are shown in Fig. 17. Indeed as expected from the characterisation techniques, no significant changes were obtained in catalytic activity. Notably, the 50 ml catalyst is the least active, as expected from analysis. An increased butadiene yield for the 100 ml catalyst has to be pointed out, but this was ascribed to an experimental error.

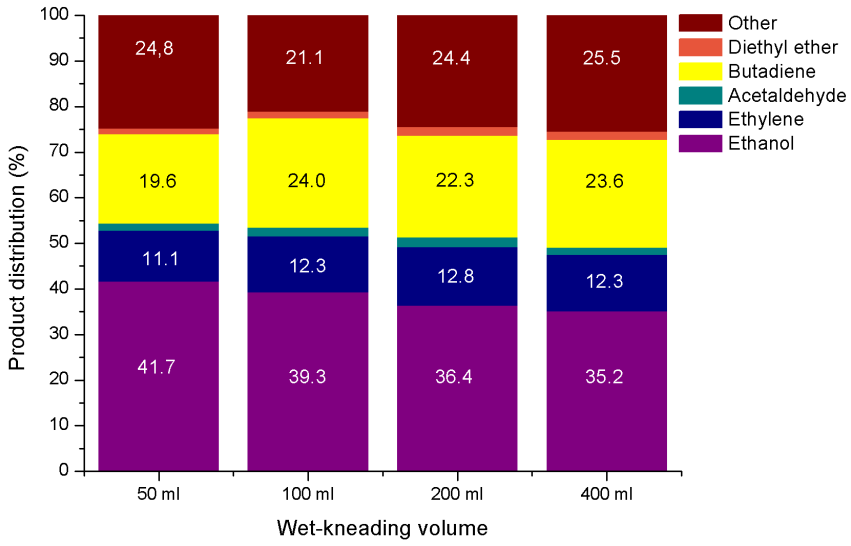

Fig. 17. *Product distribution of the catalysts with different wet-kneaded volume. The catalytic data were obtained after 4 h on stream.*

4.3.3 Wet-kneading time variation

Variation of the wet-kneading time was particularly of interest, as the formation of magnesium silicates could be followed. Fig. 18 shows the TEM images of the wet-kneaded catalysts with varied wet-kneading times.

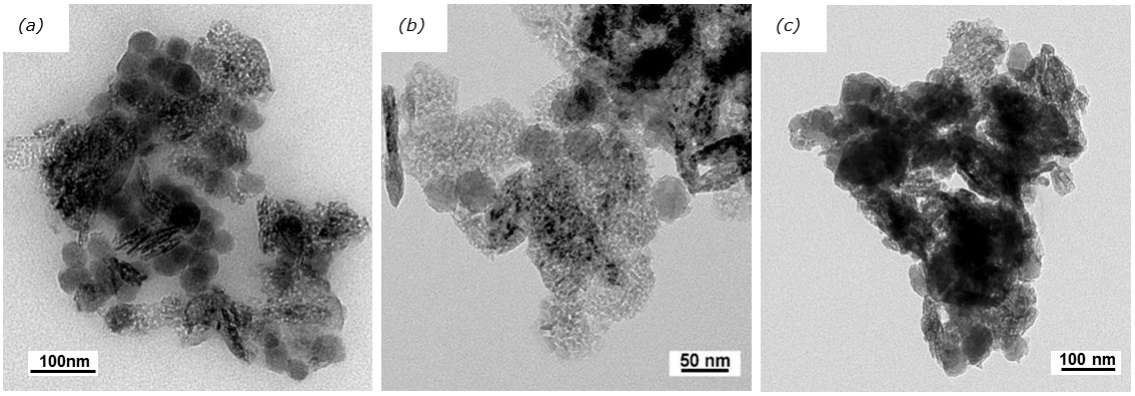

Fig. 18. *TEM images of the SiO_2-nMgO catalysts wet-kneaded for (a) 0.5 h, (b) 4 h and (c) 168 h.*

As can be seen from the TEM images and remembering the smooth surfaces of both SiO_2 and MgO precursors, the morphology of the catalyst changed during wet-kneading. This shows that deposition of dissolved species occurs during wet-kneading, with increased deposition for longer wet-kneading times. EDX maps of these catalysts depicted in Appendix 6 and 8 confirm that severe cross-deposition occurs for longer wet-kneading times, with Si deposited on top of Mg rich areas and vice versa.

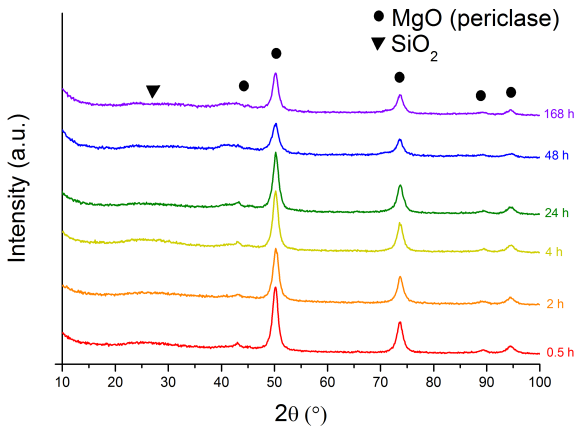

Fig. 19. *XRD patterns of the SiO_2-nMgO catalysts with different wet-kneading time.*

Table 1. *MgO peak height and particle size of the SiO_2-nMgO with different wet-kneading time obtained by using the Scherrer equation.*

Wet-kneading time (h)	MgO (200) intensity (a.u.)	MgO particle size (nm)
0.5	50.8	8.3
2	41.3	7.9
4	46.4	8.7
24	45.7	8.5
48	22.4	7.6
168	29.4	8.3

Fig. 19 shows the XRD patterns for the catalysts with different wet-kneading time. After half an hour of wet-kneading, more intense peaks are obtained, because of less cross-deposition occurring. For the first 24 h of wet-kneading, no clear trends can be observed, but after longer wet-kneading times the intensity of the MgO periclase phase dropped significantly. The Scherrer equation was used to calculate the particle size:

$$d = \frac{K\lambda}{\beta \cos(2\theta)}$$

with d the particle size in nm, K the shape factor (0.9, arbitrary units), λ the wavelength in nm, β the peak's full width at half maximum intensity (FWHM) in radians and θ the Bragg angle. Being the most intense signal, the MgO (200) peak around 2θ = 52 ° was used for calculations. The calculated particle size for the SiO_2-nMgO catalysts with different wet-kneading time are given in Table 1. Remarkably, the particle size does not change significantly during wet-kneading, with the differences attributed to measurement errors. This indicates that cross-deposition occurs delicately, not affecting the particle size.

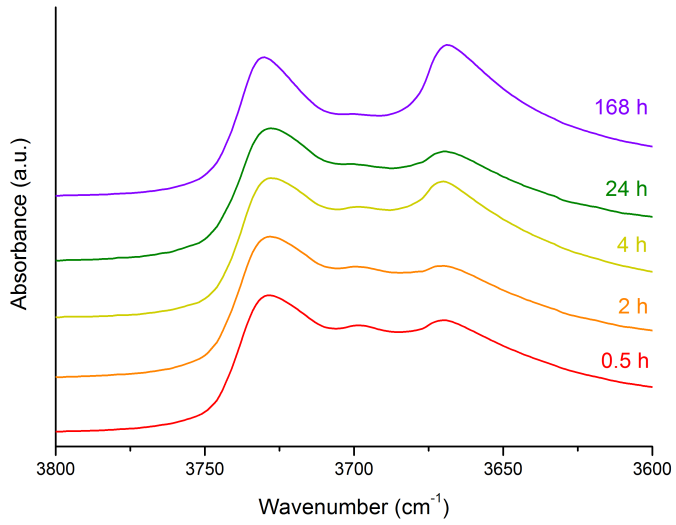

Fig. 20. *IR spectra of the SiO_2-nMgO catalysts with varied wet-kneading time. The spectra are offset, for clarity.*

Fig. 20 shows the IR spectra of the time varied catalysts. The IR spectrum of the catalyst wet-kneaded for 48 h was left out, as it showed an inconsistent result in the obtained magnesium silicate vibration at 3670 cm^{-1}. Subsequent NMR analysis proved that the IR spectrum showed an incorrect amount of magnesium silicates and was therefore discarded. As can be seen, the typical magnesium silicate band at 3670 cm^{-1} is again obtained, with different intensities for longer wet-kneading times. It was proposed that this band would increase over longer wet-kneading time. This was not the case, with a possible explanation being that different types of magnesium silicates are formed. This causes peak broadening, rather than an increased intensity of the magnesium silicate band maximum. However, IR cannot give quantitative

analysis of the different magnesium silicate phases present. Therefore, ^{1}H-^{29}Si cross polarised - magic angle spinning (CP-MAS) NMR was performed. To illustrate, the NMR spectra of the SiO_2-nMgO catalyst wet-kneaded for 4 h and Stöber SiO_2 are given as an example (Fig. 21).

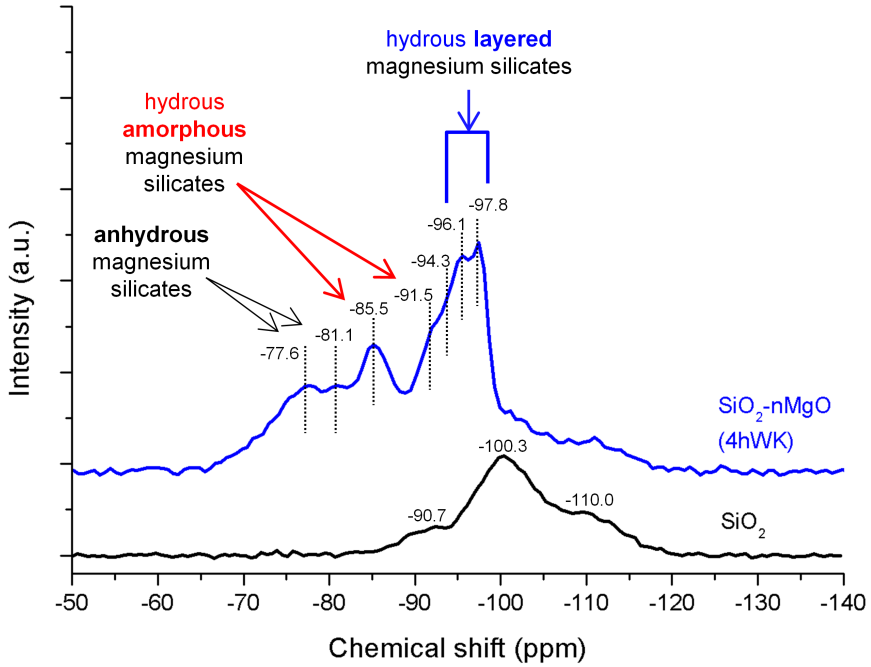

Fig. 21. *^{1}H-^{29}Si CP-MAS NMR spectrum of the wet-kneaded SiO_2-nMgO catalyst (4 h wet-kneading time) in blue and Stöber SiO_2 in black.*

The NMR spectrum of SiO_2 shows the presence of three signals. These are known to originate from silicon atoms fully surrounded by siloxane bridges (Q^4, -110.0 ppm), with one hydroxyl group (single silanol, Q^3, -100.3 ppm) or two hydroxyl groups (geminal silanol, Q^2, -90.7 ppm).[61] The NMR spectra of the wet-kneaded catalyst were manually deconvoluted, keeping the peak width and position constant. An example of the obtained results is depicted in Fig. 22, the full spectra are shown in Appendices 23-28. In these deconvolutions, Q^2, Q^3 and Q^4 were all present, but new signals are obtained as Fig. 21 depicts. These were assigned to hydrous and anhydrous magnesium silicates. From the deconvolution, the peaks of -77.6 and -81.1 ppm were assigned to anhydrous magnesium silicates, with the former being an intermediate between forsterite and enstatite;[62] and the latter ringwoodite, which is a polymorph of forsterite.[63] The hydrous magnesium silicates can be divided into two classes: hydrous amorphous and hydrous layered magnesium silicates, with the latter implying a certain degree of crystallinity. Little is known about the structure of the layered amorphous magnesium silicates, but the two signals at -85.5 and -91.5 ppm were ascribed to a silicon atom bound to a hydroxyl group and a magnesium atom (Q^3) and a silicon atom surrounded by two magnesium atoms (Q^2).[64] Finally, the signals at -94.3, -96.1 and -97.8 ppm are ascribed to the hydrous layered magnesium silicates lizardite,[65] stevensite[66] and talc.[67]

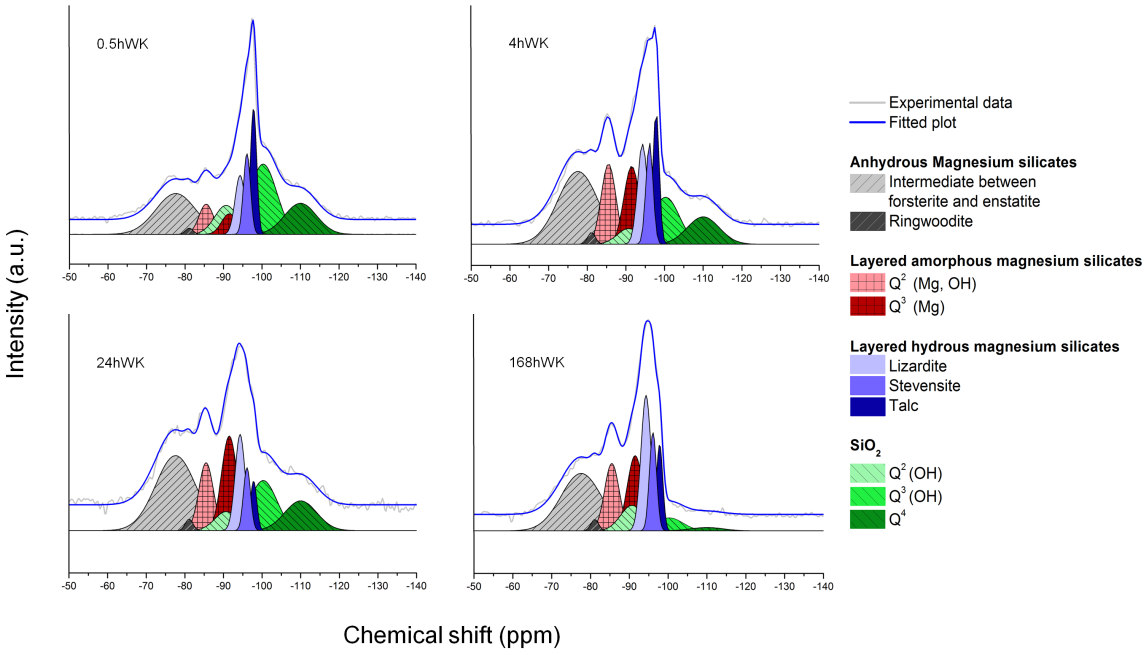

Fig. 22. *Deconvoluted NMR spectra of the wet-kneaded catalyst with varied wet-kneading time.*

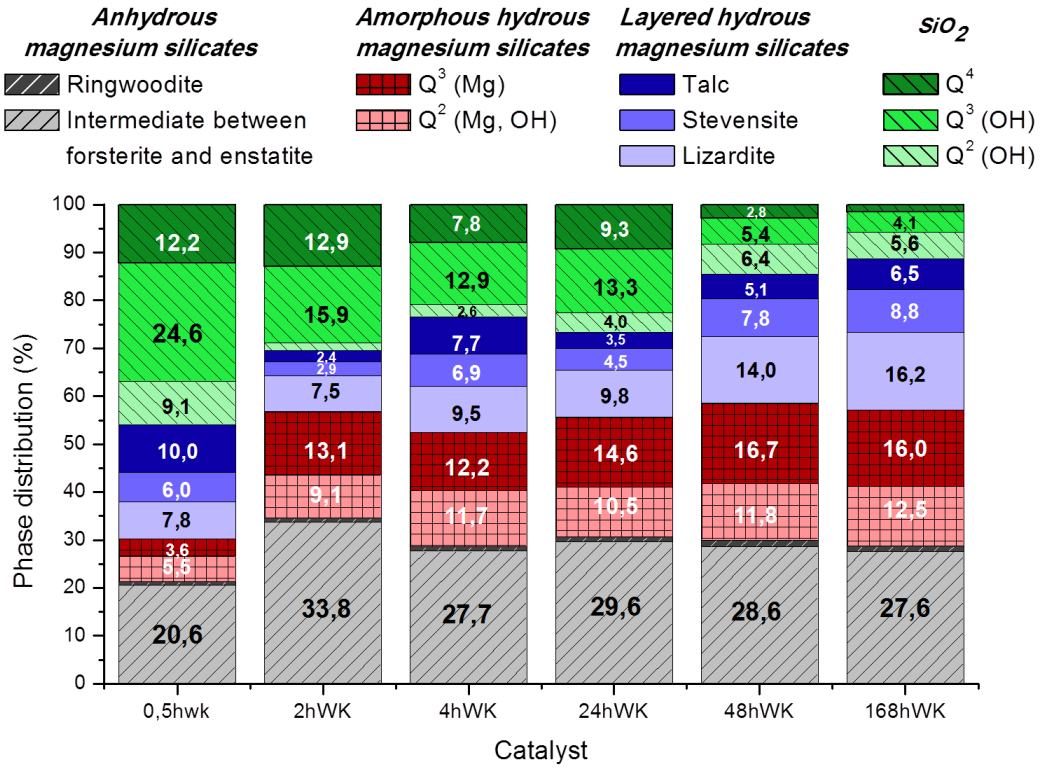

Fig. 23. *Phase distribution of the wet-kneaded catalyst with varied wet-kneading time.*

The amount of phases present after wet-kneading varied significantly over wet-kneading time, with the phase distribution depicted in Fig. 23. The phase distribution was obtained from the peak area of the deconvoluted Gaussian functions, compared to the total peak area in the deconvoluted spectra. It has to be emphasised that these numbers are not implying a concentration of phases of some sort, since the peak areas increase for longer wet-kneading time. Therefore, these numbers do not give a quantitative amount of magnesium silicates present, but rather the amount of phases present compared to the other present phases in that catalyst. Nonetheless, Fig. 23 clearly depicts an increase of total magnesium silicates (grey, red and blue) compared to pure silica (green). Furthermore, when compared to Figure 20, Fig. 23 shows the same trend in total amounts of magnesium silicates: the total amount increases until 4 h, slightly decreases for the 24 h wet-kneaded catalyst and increases again for even longer wet-kneading times. To emphasise, NMR data of the 2 h wet-kneaded catalyst showed a larger amount of magnesium silicates present compared to what IR indicated. This was ascribed to the difference in magnesium silicate phases, contributing differently to the vibrations in IR. The low amount of magnesium silicates present in the catalyst wet-kneaded for 24 h was ascribed to an experimental error.

Catalytic testing results are shown in Fig. 24 and 25. Again, no clear trends are observed from the product distribution, but the selectivity towards butadiene was decreased, while the ethylene selectivity increased.

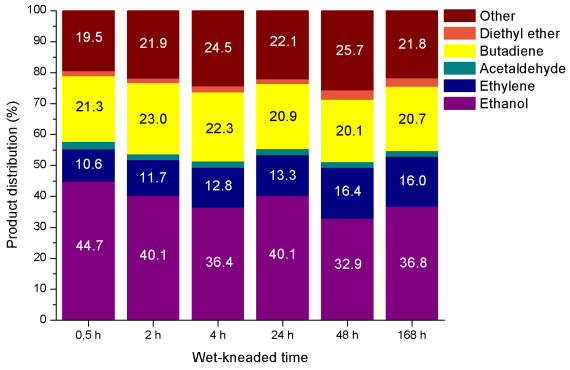

Fig. 24. *Product distribution ofthe SiO_2-nMgO catalysts with different wet-kneading times.*

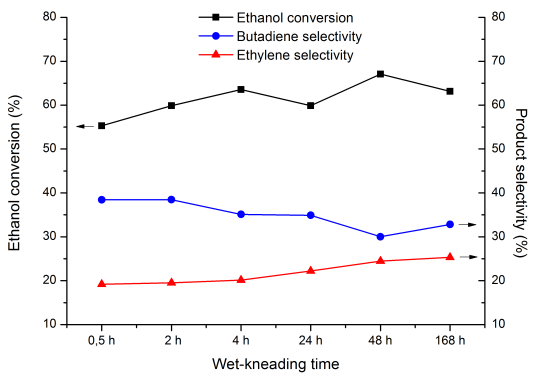

Fig. 25. *Butadiene and ethylene selectivity of the SiO_2-nMgO catalysts with varied wet-kneading times.*

Chung et *al.* found a correlation between the hydrous amorphous magnesium silicates with the ethylene yield and the hydrous layered magnesium silicates with the butadiene yield.[43] For the SiO_2-nMgO catalysts with different wet-kneading times, Fig. 26 and 27 show correlation graphs between the peak area of these magnesium silicates and the butadiene and ethylene yields.

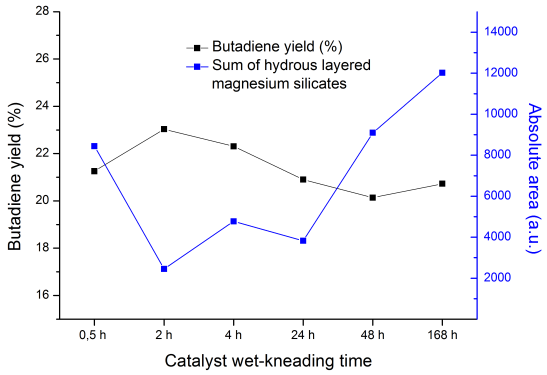

Fig. 26. *Butadiene yield and the sum of absolute peak area of hydrous layered magnesium silicates for the SiO_2-nMgO catalyst with different wet-kneading time.*

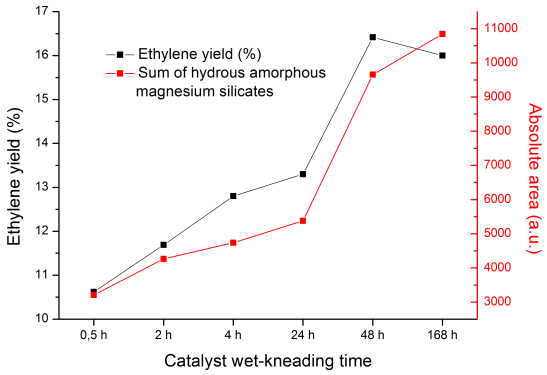

Fig. 27. *Ethylene yield and the sum of absolute peak area of hydrous amorphous magnesium silicates for the SiO_2-nMgO catalyst with different wet-kneading time.*

From Fig. 26, no clear correlation can be observed. This could be ascribed to the strong morphological changes for wet-kneading times, as seen in the TEM images of Fig. 18a-c and the EDX maps in Appendix 6 and 8. Because of the severe cross deposition, it is not unlikely that other surface species essential for catalysis are blocked, such as MgO for MPV reduction or aldol condensation. As mentioned before, pure talc does not show significant activity. A mixture of talc and MgO however is active, albeit highly selective towards butanol. Furthermore, reactants crossing the catalyst bed can interact with various surface species, leading to side reactions and possibly blocking of the surface, but also the absence of the correct surface species in close vicinity needed for the next catalytic step can influence the product distribution. Therefore, it is suggested that a delicate balance between surface species is needed for the Lebedev process. This problem could be resolved by a dual-bed reactor, where the reactants cross the active sites in the right order. However, the active sites of the wet-kneaded catalysts first need to be clarified and isolated, in order to perform catalytic testing in such a setup. To elaborate, it is still unknown what the exact role of the layered magnesium silicate species is in the mechanistic steps seen in Fig. 5. Subsequently, once all essential species have been isolated, kinetic testing can be carried out to determine which species contribute to which step in the Lebedev mechanism (Fig. 5).

Notably, Fig. 27 does show a clear correlation between the hydrous amorphous magnesium silicates and ethylene yield. In Chapter 2.1, it was stated that the catalyst needs acidic sites for dehydration reactions, presumably supplied by SiO_2. Therefore, NH_3 Temperature-Programmed Desorption (TPD) was recorded to study the difference in acidic sites present. Fig. 28 shows the obtained profiles and Table 2 gives the resulting total amount of acid sites.

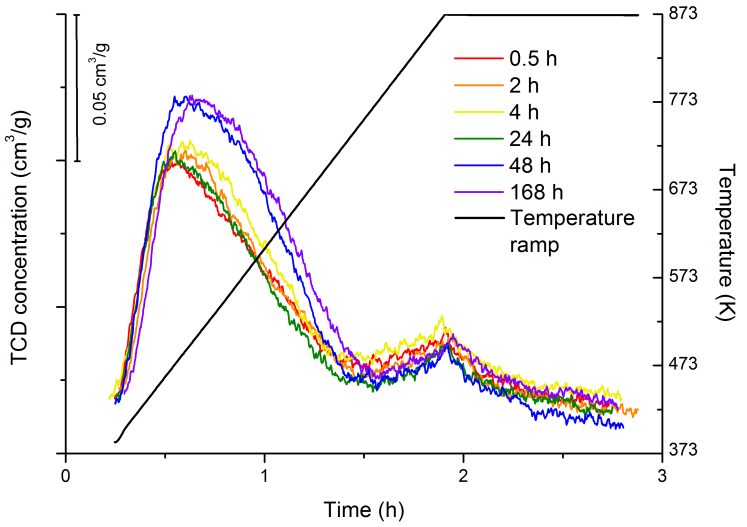

Fig. 28. *NH_3-TPD profiles for the SiO_2-nMgO catalyst with different wet-kneading time. The black line shows the temperature at which desorption takes place.*

In Fig. 28, the signal desorbing at lower temperatures originates from acidic sites with intermediate strength and the signal desorbing at higher temperatures from strong acid sites.[28] No significant differences in the acidity are observed with TPD for longer wet-kneading time, except for 48 and 168 h (Table 2). The total amount of acid sites gives similar results compared to related materials,[28] but no clear trend in acidity is observed. The selectivity towards ethylene increased however
(Fig. 25 and 27), as it was stated that the acid sites are responsible for ethanol dehydration. Furthermore, the ethylene yield does not correlate to the total amount of acid sites. Knowing that pure SiO_2 is not active in ethanol conversion, this result is in line with the hypothesis that the hydrous amorphous magnesium silicate species are responsible for the undesired ethylene production. Still, more analysis needs to be performed on these species. The structure of amorphous magnesium silicates remains unresolved[64] and it is uncertain if these species are responsible for e.g. the acidity of the catalyst. Again, the amorphous magnesium silicate species first need to be isolated to confirm the hypothesis about their role in the Lebedev process.

Table 2. *Total amount of acidic sites of the SiO_2-nMgO with different wet-kneading time, as obtained from NH_3-TPD.*

Catalyst wet-kneading time (h)	Total acid sites (mmol/g)
0.5	0.235
2	0.215
4	0.253
24	0.222
48	0.295
168	0.281

4.3.4 Influence of NH_4NO_3 during wet-kneading

As mentioned before, the pH fluctuates during wet-kneading due to a difference in dissolved species. Therefore, the addition of a buffer was added to investigate the effect of pH variations during wet-kneading. This could possibly lead to the formation of a specific magnesium silicate phase. NH_4NO_3 was chosen as a buffer, as has been used in the preparation of related materials and analysis of formed magnesium silicates to prevent severe pH fluctuations.[64] Furthermore, the capability of completely removing the buffer during calcination makes NH_4NO_3 an advantageous compound for addition to wet-kneading compared to other buffers. The effect of NH_4NO_3 addition on the pH is shown in Fig. 29.

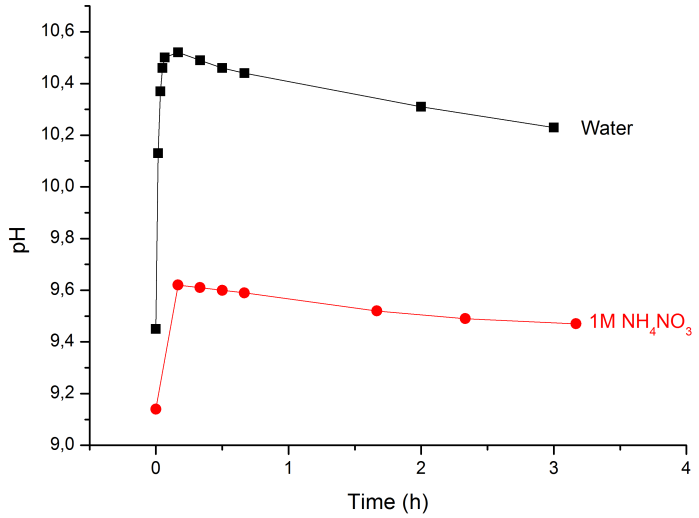

Fig. 29. *pH values during wet-kneading of SiO_2-nMgO wet-kneaded in water (black) and in 1 M NH_4NO_3 (red).*

The same pH trends observed by Chung et *al.* were obtained when SiO_2 and MgO were wet-kneaded, due to a difference in dissolved species (see Chapter 2.2).[43] Keeping the pH stable was not obtained when NH_4NO_3 was added during wet-kneading, as the same decrease in pH was obtained during standard wet-kneading conditions. The pH decreased however, which could have a influence on the precursor solubility. However, the MgO periclase phase was completely removed from the catalyst, as can be seen in the XRD patterns of Fig. 30.

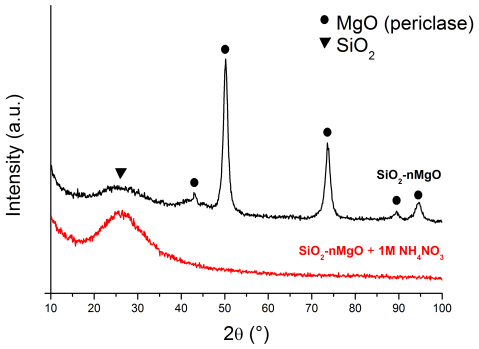

Fig. 30. XRD patterns of the SiO_2-nMgO catalyst wet-kneaded in water (black) and in 1M NH_4NO_3 (red).

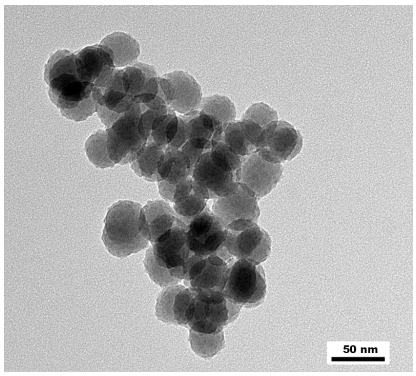

Fig. 31. TEM image of the SiO_2-nMgO catalyst wet-kneaded in 1M NH_4NO_3.

This was confirmed by TEM analysis (Fig. 31); the MgO domains were not observed. The NH_4NO_3 present during wet-kneading dissolved $Mg(OH)_2$ species,[68] leaving corrugated SiO_2 spheres, with a decreased particle size of approximately 33 nm.
Looking at the product distribution in Fig. 32, a high fraction of unreacted ethanol is still found in the product mixture. However, it can be seen that a high selectivity towards ethylene is obtained.

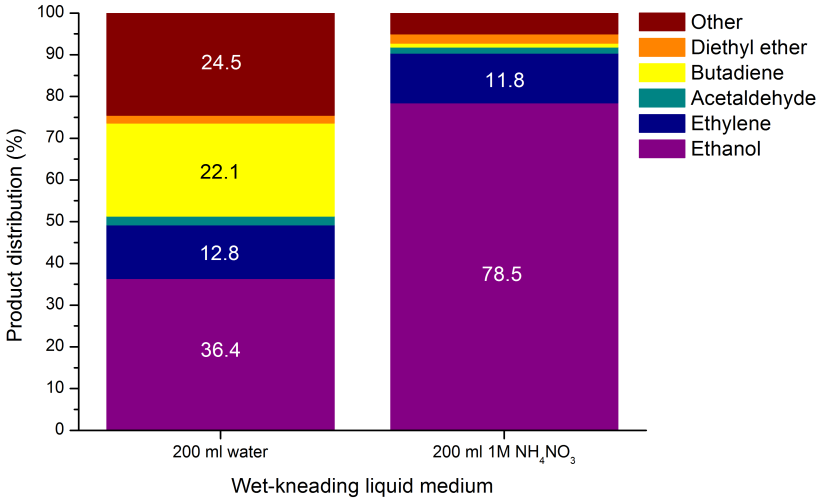

Fig. 32. Product distribution of the SiO_2-MgO catalyst wet-kneaded in water (left) and in 1M NH_4NO_3 (right).

It has to be emphasised that the hydrous amorphous magnesium silicates are thought to be responsible for ethylene formation as was stated in Chapter 4.3.3. Since $Mg(OH)_2$ dissolved during wet-kneading, it is possible that magnesium species precipitated on top of SiO_2, forming magnesium silicates. Fig. 33 shows the postulated mechanism for magnesium silicate formation.

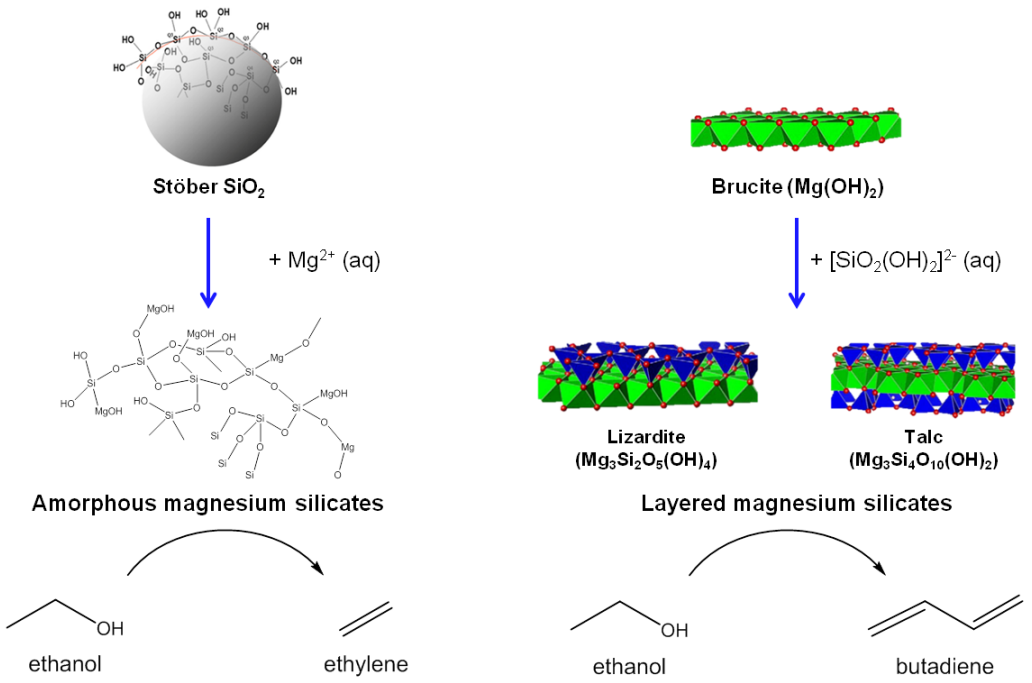

Fig. 33. *Proposed mechanism for the formation of amorphous and layered magnesium silicates and their designated role in the Lebedev process. The amorphous magnesium silicate structure was estimated for illustrative purposes.*

As stated in Chapter 2.2, due to the differences in surface charge, it is proposed that magnesium species are deposited on the SiO_2 surface and silicon species on the $Mg(OH)_2$ surface. As Fig. 33 depicts, it is assumed that due to the higher degree of crystallinity of the $Mg(OH)_2$ brucite phase, the crystalline hydrous layered magnesium silicates are formed on top of $Mg(OH)_2$ and anchored after calcination. In brucite, the Mg^{2+} ions have an octahedral symmetry, which is the same in hydrous layered magnesium silicates, such as lizardite or talc.[37,43] Moreover, it is therefore assumed that the amorphous magnesium silicates are formed on the amorphous SiO_2 surface.

Since $Mg(OH)_2$ fully dissolved after addition of NH_4NO_3, there are no domains present to form layered magnesium silicates. Therefore, it is assumed that solely amorphous magnesium silicates have been formed on top of the SiO_2 surface, which is presumably the cause for the highly selective catalyst towards ethylene. FT-IR spectroscopy (Fig. 34) shows that the addition of NH_4NO_3 does not yield pure SiO_2 vibrations, but a large signal consisting of different vibrations. Most likely, the signal consists of magnesium silicates as well, as the IR spectra seem to correlate. This has to be verified by NMR, to see which magnesium silicate phases are present. If NMR shows the sole presence of amorphous magnesium silicates, the hypothesis is proven.

Concluding, the wet-kneading parameters were optimised in terms of wet-kneading precursor variation, amount of water present during wet-kneading and wet-kneading time variation. It appears that the reference catalyst (wet-kneading of Stöber SiO_2 and nMgO in 200 ml water for 4 h, 600 rpm) still gives the optimal performance in terms ethanol conversion and butadiene yield. Therefore this catalyst was chosen as a support for promoter impregnation studies.

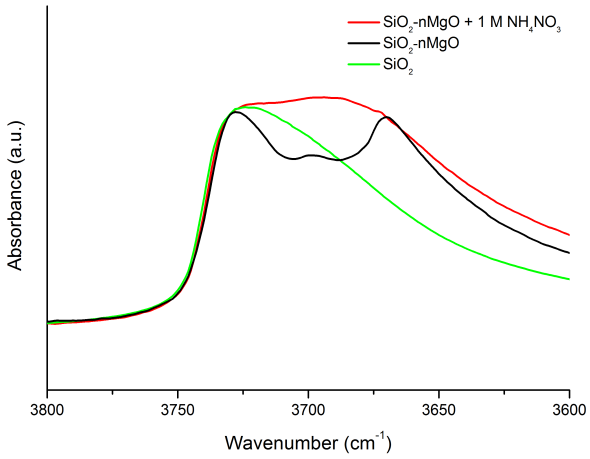

Fig. 34. *FT-IR spectra of SiO_2 (green) and the SiO_2-MgO catalysts wet-kneaded in water (black) and in 1M NH_4NO_3 (red).*

4.4 Conclusion

The wet-kneading parameters were optimised. Altering the wet-kneading volume did not influence the catalytic activity significantly. When $MgSO_4 \cdot 7\,H_2O$ was used as feedstock for $Mg(OH)_2$ instead of $Mg(NO_3)_2 \cdot 6\,H_2O$, needle-like "sMgO" nanoparticles with a smaller size than the platelet-shaped "nano"MgO were obtained. The wet-kneaded SiO_2-sMgO caused an increased ethanol conversion, but the catalyst deactivated faster compared to wet-kneaded SiO_2-nMgO. The product selectivity towards ethylene and butadiene remained unchanged, but decreased faster over time as well. ICP-OES measurements confirmed the presence of residual sulphur in the precursor, which could affect the catalyst activity. However, the reactor gave an unstable ethanol flow when testing the wet-kneaded SiO_2-sMgO catalyst.
Varying the wet-kneading time proved insightful, as the formation of magnesium silicates could be followed. A difference in product selectivity was obtained. This was attributed to the different magnesium silicates being catalytically relevant. FT-IR results showed that the amount of magnesium silicates seemed to correlate to the catalytic activity, but the typical signal at 3670 cm^{-1} was not sufficient to identify the different phases of magnesium silicates formed. ^{1}H-^{29}Si CP-MAS NMR showed that the hydrous amorphous magnesium silicates correlate to the detrimental ethylene formation. The hydrous layered magnesium silicates were postulated to correlate to the butadiene yield, but no clear correlation was obtained, presumably caused by the absence or blockage of essential surface species of e.g. MgO.
Keeping the pH constant during wet-kneading by addition of NH_4NO_3 was attempted, but this caused a dissolution of the $Mg(OH)_2$ species, preventing the formation of layered magnesium silicates, assumed to be essential for butadiene formation. A highly selective catalyst towards ethylene was obtained, which could be caused by the presence of amorphous magnesium silicates.

5 Impregnation of the Lebedev catalyst

5.1 Introduction

It has been shown that CuO addition to the wet-kneaded catalyst as a promoter further increased the ethanol conversion and butadiene selectivity significantly. It was believed that CuO influenced the dehydrogenation of ethanol, shifting the rate determining step from acetaldehyde formation to aldol condensation towards 3-hydroxybutanal.[17] However, the catalyst suffered from severe carbonaceous deposition. Therefore, more metal oxides were loaded on the catalyst to possibly increase the catalyst stability, activity and selectivity rates.

5.2 Experimental procedure

5.2.1 Materials

For the chemicals used for the reference wet-kneaded SiO_2-nMgO catalyst, which was used as support, please refer to 4.2.1. Metal nitrates or ammonium metallates were chosen for impregnation to prevent possible contamination of unremovable counterions, with the following chemicals used:

$Fe(NO_3)_3 \cdot 9\,H_2O$ (99%, for analysis, Acros); $Ni(NO_3)_2 \cdot 6\,H_2O$ (99%, for analysis, Acros); $Co(NO_3)_2 \cdot 6\,H_2O$ (99%, for analysis, Acros); $AgNO_3$ (99.9%, trace metals basis, Alfa Aesar); $ZrO(NO_3)_2 \cdot H_2O$ (99.99% trace metals basis, Sigma-Aldrich); $Zn(NO_3)_2 \cdot 6\,H_2O$ (Aldrich); $Pt(NO_3)_2 \cdot 4\,NH_3$ (99.99%, trace metals basis, Sigma-Aldrich); $Mn(NO_3)_2 \cdot 4\,H_2O$ (99%, for analysis, Acros); $Ru(NO)(NO_3)_3$ (99.99%, Ru 31.3% min, Alfa Aesar); $Pd(NO_3)_2 \cdot 4\,NH_3$ (10% in water, Sigma-Aldrich); $(NH_4)_6Mo_7O_{24} \cdot 4\,H_2O$ (99.99%, trace metals basis, Sigma-Aldrich) and $Cu(NO_3)_2 \cdot 3\,H_2O$ (98%, ACS reagent, Sigma-Aldrich).

5.2.2 Catalyst preparation

The preparation of the reference wet-kneaded Lebedev catalyst is described in detail in Chapter 4.2.2. To promote the catalyst with transition metals, the incipient wetness impregnation technique was used. A loading of 1% of metal oxide species was attempted. 0.5 g of the wet-kneaded SiO_2-nMgO catalyst was evacuated and mildly heated for 1 h. The metal salt was dissolved in water and the desired volume was added drop wise to the evacuated catalyst under vigorous stirring. After impregnation, the catalyst was stirred for 1 h. Finally the catalyst was held under vacuum over night. The obtained product was calcined for 5 h at 773 K.

5.2.3 Catalyst testing

0.12 g quartz wool and 0.2 g catalyst (sieved to 90-425 μm) were put in a quartz glass reactor. The reactor was heated to 698 K and left for 1 h as pretreatment. The amount of ethanol introduced to the reactor was controlled via a Shimatzu LC pump. 0.01 ml min^{-1} liquid ethanol was flowed through the reactor with 98 ml min^{-1} N_2 as carrier gas, yielding 2.15 vol. % ethanol in the gas phase mixture. The analysis of the reaction mixture was performed by means of

GC-FID using a CP poraplot Q-HT column; quantification of the main components (ethanol, ethylene, acetaldehyde, butadiene, and diethyl ether) was based on calibration curves obtained by feeding known amounts of the various compounds.

5.2.4 Characterisation

Fourier transform infrared spectroscopy (FT-IR) measurements were taken with 25 scans per spectrum on a Perkin Elmer System 2000 with a DTGS detector and a resolution of 4 cm^{-1}. Approximately 17 mg of the catalyst were pressed into a pellet and placed into the infrared measurement cell. The catalyst was dried in the cell under vacuum with a temperature ramp of 5 K min^{-1} reaching the desired temperature of 823 K; FT-IR spectra were taken every 25 K in the temperature range 323-823 K. Once 823 K was reached, this temperature was kept constant for 30 min; spectra were taken at 5, 10 and 30 min after reaching the maximum temperature.
Textural properties of the reference wet-kneaded catalyst were studied by N_2 physisorption measurements at 77 K using a Micromeritics Tristar 3000. Prior to the adsorption measurements the samples were dried at 573 K for 12 h. The Brunauer-Emmett-Teller (BET) method was applied to calculate the total surface area. The t-plot method was applied to obtain the micropore volume and external surface area. The Barrett-Joyner-Halenda (BJH) model was used to determine the size of the mesopores.

5.3 Results and discussion

Table 3. *N_2-physisorption results for the wet-kneaded catalyst and the wet-kneaded catalyst promoted with iron.*

Catalyst	Surface area (m^2/g)	Pore volume (cm^3/g)	Micropore volume (cm^3/g)	Pore size (nm)
SiO_2-nMgO	190.8	0.80	0.005	15.1
Fe_3O_4/SiO_2-nMgO	173.9	0.62	0.012	11.2

N_2 physisorption results are given in Table 3. It can be seen that the wet-kneaded catalyst is not highly porous, with a negligible amount of the total pore volume consisting of micropores. This can be seen in the adsorption and desorption isoterms as well (Appendix 9), since the presence of micropores would show a sharp increase in adsorbed gas around $0<P/P_0<0.1$ in the adsorption and desorption isoterms.[69] Furthermore, hysteresis is observed between the isotherms, indicating the presence of mesopores.[69] Therefore it is assumed that due to the low porosity, diffusion limitation does not play a significant role in the catalyst. Furthermore, impregnation with iron expectedly caused a decrease in surface area and pore volume, due to the occupation of new metal species on the catalyst surface. It was assumed that this occurs for all impregnated catalysts.
After impregnation, the transition metal species could not be observed by XRD and TEM (data not shown, the same result was found by Angelici et al.[17]). However, the wet-kneaded catalyst

Table 4. *Catalyst and corresponding metal loading from ICP-OES analysis.*

Catalyst	Metal loading (wt. %)
Fe_3O_4/SiO_2-nMgO	0.64
PdO/SiO_2-nMgO	0.68
Co_3O_4/SiO_2-nMgO	0.63
MnO_2/SiO_2-nMgO	0.68
Ni_2O_3/SiO_2-nMgO	0.54
ZnO/SiO_2-nMgO	0.67
Ag/SiO_2-nMgO	0.93
PtO_2/SiO_2-nMgO	0.70
CuO/SiO_2-nMgO	0.86
MoO_3/SiO_2-nMgO	0.75
ZrO_2/SiO_2-nMgO	>0.37
RuO_2/SiO_2-nMgO	>0.21

did contain metal species, which was confirmed by Inductively Coupled Plasma - Optical Emission Spectrometry (ICP-OES) analysis shown in Table 4. Only the amount of Ru and Zr present on the promoted catalyst could not be quantitatively determined, due to an incomplete dissolution of the catalyst handed in for ICP-OES analysis. For Ag, it was assumed that it underwent thermal decomposition, resulting in metallic silver present in the catalyst after calcination,[70] but this has to be verified by e.g. EXAFS or XANES. The location of the metal species on the catalyst has unfortunately not been further analysed. EDX maps or again EXAFS or XANES could reveal the location of the metal species on the catalyst, where Angelici et *al.* showed that Cu is deposited on both SiO_2 and MgO rich areas.[17] However, NMR analysis carried out by McCarty et *al.* showed that different metal species have deviating preferences for surface sites.[62] This result is backed by later work of Angelici et *al.*, where it was shown that the postulated Cu active site was situated in an octahedrally distorted geometry, mainly present on MgO surfaces. Square planar geometry present on SiO_2 surfaces, the same geometry as for bulk CuO, showed a significant drop in catalytic activity.[71] Looking at the FT-IR spectra in Fig. 35, it can be seen that the typical magnesium silicate band slightly increased in intensity. First it was assumed that this was due to the addition of water during impregnation, again allowing cross-deposition to take place. However, when the catalyst was impregnated with water as a blank test, no significant increase of the magnesium silicate band was observed. An explanation for this increase could be the formation of new types of magnesium silicate minerals mixed with metal species. To illustrate, grunerite, $Fe_2(Fe,Mg)_5Si_8O_{22}(OH)_2$, shows vibrations at 3616 and 3617 cm^{-1}, respectively.[72] These were not obtained in the recorded spectrum seen in Fig. 35, but it is possible that the signals overlap with other broad signals. Metal phyllosillicates or orthosilicates could not be observed in FT-IR, since these vibrations are expected in in the fingerprint region, which could not be resolved due to a significant amount of noise.[73] The presence of these species could be shown by ^1H-^{29}Si CP-MAS NMR,[62] or other techniques such as EXAFS or XANES to investigate the intimacy between the metal species and the support.[71] Furthermore, metal vibrations were not observed, as these are expected in the fingerprint region as well.

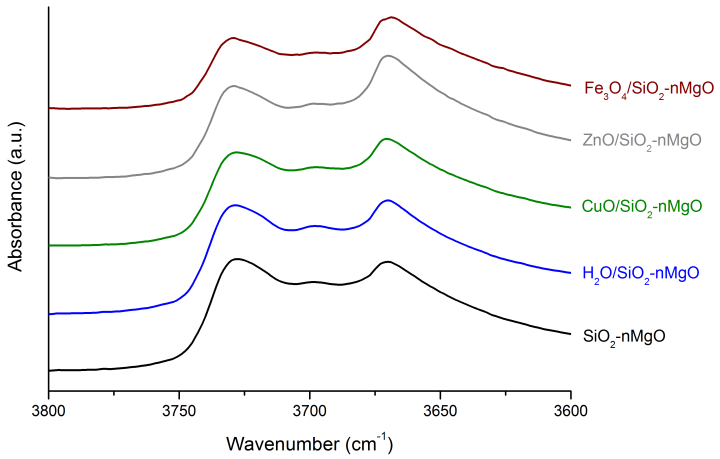

Fig. 35. *FT-IR spectra of various metal loaded SiO_2-nMgO catalysts. The observed increase of the magnesium silicate band is representative for all impregnated catalysts. The spectra are offset, for clarity.*

Catalytic testing results of the impregnated catalyst are shown in Fig. 36, with the individual catalytic performance of each catalyst - including the unpromoted catalyst - shown in Appendices 10-22. As the impregnated catalysts have not been reduced to obtain the promoter metallic species essential for dehydrogenation, it was expected that their metal oxide phase is present prior to the reaction. However, it is believed that these species get reduced in-situ by ethanol or formed hydrogen during the reaction.[71]
Due to technical malfunctions and therefore inconsistencies in the amount of ethanol observed in GC, the ethanol conversion is left out in Fig. 36. Because of this inconsistency in the ethanol signal, the selectivity towards each product could not be quantitatively obtained.
All impregnated catalysts produced traces (<5%) of butanol as a new main side-product. Most promoters have led to an increase of butadiene yield compared to the unpromoted catalyst, as observed by other work.[1,12,18,49,74,75] These authors stated that Cu, Ag and Zn promoters performed best with yields over 50 %. The same activity was observed for Cu and Ag in our case. The initial activity of Ag is higher than for Cu. This was ascribed to the presence of metallic Ag present prior to the reaction. As mentioned earlier, Ag can be reduced during calcination due to thermal decomposition of AgO. Ag therefore does not need to be reduced in situ, making Ag capable of directly promoting dehydrogenation towards acetaldehyde.
The amount of acetaldehyde produced increased for all catalysts, compared to the unpromoted catalyst. Furthermore, it is visible that Zn promotion yields significantly more acetaldehyde, meaning that the rate determining step has shifted from the dehydrogenation to the aldol condensation step. As the low butadiene yields indicates, it could be possible that the Zn is deposited on the sites responsible for aldol condensation, or that Zn is mainly capable of facilitating dehydrogenation.[55] As for Mo promotion, it can be seen that although butadiene yield decreases rapidly, the acetaldehyde yield remains constant. This indicates that Mo catalyses dehydrogenation towards acetaldehyde, but the aldol condensation step is now limited severely. Compared to Zn, the same explanation could be given, since Zn promotion led to a similar product distribution. But this does not explain the initial high selectivity towards butadiene. Perhaps Mo contains a more beneficial crystalline geometry than Zn.

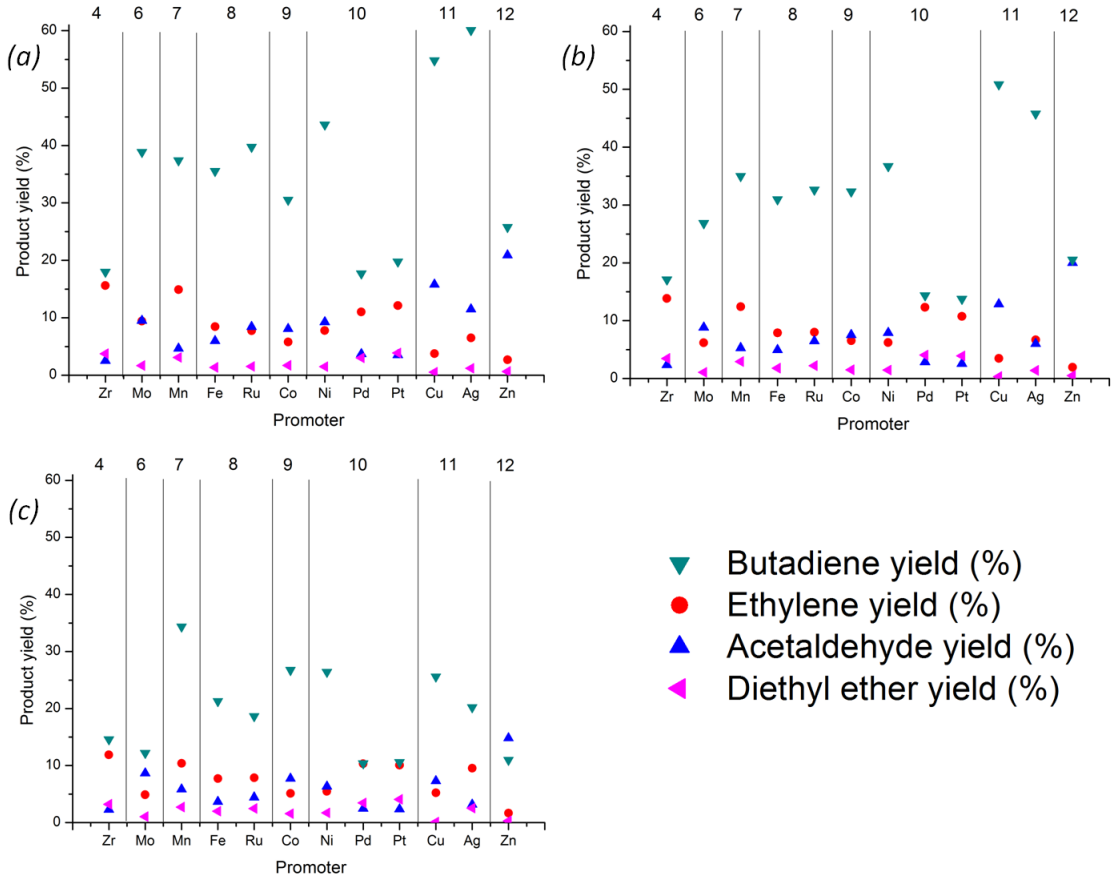

Fig. 36. *Catalytic results of the impregnated catalysts after (a) 0.5h, (b) 4h and (c) 24h on stream. The numbers on top of the graphs correspond to the element group in the periodic table.*

A clear volcano plot was unfortunately not obtained, so the selectivity does not seem to directly depend on the electronic structure of the metals. Further research needs to be carried out on these catalysts, as it is uncertain in what form the metal species are (metals, metal oxides, phyllosylicates or mixed with magnesium silicates).
Remarkably, Pt and Pd impregnated catalysts showed significant lower activity compared to the other catalysts, where it was postulated that these catalysts would be highly selective towards butyraldehyde or butanol.[34] An explanation could be that the activity of these promoters decreases as elements in lower rows in the periodic table are used, as Ni does show decent activity towards butadiene. In this case, the atomic size perhaps influenced the activity difference. But this does not seem to hold for other promoters in the same group. For instance Ru and Ag show higher initial activity compared to Fe and Cu, respectively. In addition, Pt shows higher initial activity than Pd. It would then seem that Pd and Pt are not activated in-situ and an additional reduction step is required for these catalysts, or that the correct crystal plane capable of (de)hydrogenation is not present.
Ru promotion was believed to decrease the catalyst activity, as it showed small activity in

crotonaldehyde transformation, which actually further decreased when Mg was added.[76] An increase of initial butadiene selectivity was observed, however. Bachiller-Baeza et *al.* used a severe reduction method, which could have deactivated the catalyst, prior to the reaction. Possibly the in-situ reduction during the gas-phase reaction is more beneficial for Ru to yield an active catalyst.
Most catalysts suffered from severe carbonaceous deposition, compared to the unpromoted catalyst (Appendix 10). Angelici et al. ascribed this as a main cause for the observed deactivation of the Cu impregnated wet-kneaded catalyst, but it was not stated if the carbonaceous compounds formed on the metal surface or on the support.[1] A possible explanation for the deactivating behaviour could be the formation of carbonaceous compounds and subsequent migration to the promoter surface, causing blockage of the metal species.[77] To prevent carbonaceous compounds from forming, Ezinkwo et *al.* added H_2O_2 as a "process initiator", which resulted in a longer catalyst lifetime[78]
To emphasise, as previously mentioned in Chapter 5.2.1, (ammonium) metal nitrate complexes or ammonium metallates were chosen as precursors for impregnation. However, the chemicals were not of the same purity, which could mean that contamination weres present, further influencing the deactivating behaviour. ICP-OES analysis confirmed the presence of other metal species, with the largest impurity originating from Fe. For future work, it is advisable to purchase the same chemical grade. Unfortunately, not all of these chemicals were present.
Secondly, the Ag catalyst deactivated faster compared to the Cu catalyst. Perhaps there are impurities present in the Ag catalyst. Furthermore, not all catalysts deactivated as severely as the Cu and Ag catalysts. The most stable catalyst was obtained with a Mn promoter. It is known that Mn promotion can increase the catalyst stability and resistivity against coke formation.[79] As is known for reforming catalysts, carbonaceous compounds poison the catalytic surface by forming large graphenic sheets. These sheets need a free ensemble of surface atoms in order to form. This ensemple can be distorted by e.g. transition metals, increasing the coke resistivity of the catalyst.[80] This argumentation however does not seem to hold, as only Mn and Zr does not show severe deactivation. Secondly, some carbonaceous compounds have been formed on these catalysts as well, albeit less abundant than for the other catalysts. Furthermore, the produced catalysts in this work are thought to lack high ordering because of the disappearance in TEM and XRD. Ordering is a prerequisite for the stated ensemble needed for carbonaceous sheets to form. Thus, it seems that it is more likely that migration of the carbonaceous compounds does not occur as abundant on Mn, compared to the other impregnated catalysts. Furthermore, the same increase of butadiene selectivity was observed for Mn promoted sepiolite as Kitayama et *al.*[74] Where they found that the ethylene yield slightly decreased, the same amount of ethylene was obtained compared to the unpromoted wet-kneaded catalyst. This could be due to the postulated responsibility of the amorphous magnesium silicates. On the contrary, the ethylene selectivity decreased for the other impregnated catalysts, meaning that those promoters are more effective in the competitive dehydrogenation versus dehydration reactions.
Zr is known to enhance the activity in the Ostromislensky process, c.q. when a mixture of ethanol and acetaldehyde is used as feedstock, as reported by Han et *al.*[81] However, the same authors observed a severe decrease of butadiene yield and a high selective ethylene selectivity when solely ethanol was brought in contact with the catalyst. Compared to the reference catalyst, a drop in butadiene and an increase in ethylene production is observed as well, albeit

not as severe described by Han et *al.*
For a complete dataset, more transition metals need to be promoted on the wet-kneaded catalyst. Elements as Ir,[32] Cr and Ta,[82] Nb,[83] Ti[84] and Hf,[19,84] but also Au[31] are believed to give good results in intermediate steps or the complete reaction of the Lebedev process. Furthermore, Ga is often used as a dehydrogenation promoter in the conversion of paraffins and olefins to aromatics,[85,86] possibly circumventing ethylene formation. Secondly, Ce shows high selectivity towards crotyl alcohol in the conversion of crotonaldehyde,[76] so lanthanoids and actinoids could be regarded as possible candidates for further promotion. When the complete dataset is obtained, increasing metal loadings of well performing promoters[75] and alloying[19,35,39,87–89] are the next steps for research on the promotion effects of the wet-kneaded catalyst. Some metals did not show a significant improvement or actually decreased catalytic activity, but perhaps its beneficial properties are boosted in combination with another metal. For example Mn addition to Cu or Ag could possibly produce a more coke resistant catalyst. Furthermore, a Pt-Co alloy has been widely used in the selective hydrogenation of α-β unsaturated aldehydes.[90,91]
Finally, Angelici et *al.* showed that the manner of introducing the promoter to the wet-kneaded catalyst can alter the catalytic performance. For example, impregnating the individual components prior to wet-kneading yield differenct catalytic behaviour than impregnation after wet-kneading.[71] This result should be reproduced. Furthermore, other loading techniques such as e.g. physically mixing the metal with the wet-kneaded catalyst could possibly lead to different selectivities. Techniques involving the resuspension of the catalyst in water, such as ion-exchange or deposition-precipitation should be avoided, as these will influence the amount and composition of magnesium silicates as well.

5.4 Conclusion

The wet-kneaded catalyst was successfully impregnated with various transition metals. Literature stated that the catalysts are reduced in situ, yielding metallic species capable of dehydrogenation. Of these catalysts, Cu and Ag promotion gave the highest catalytic performance, with high butadiene selectivities obtained. Pt and Pd catalysts were remarkably lower in activity, ascribed to an insufficient in-situ reduction of the catalyst or an incorrect metal phase present. Most catalysts suffered from deactivation, presumably caused by severe carbonaceous deposition. Mn yielded a moderate increase of butadiene yield, but a high stability was observed.
Further analysis on these catalysts has to be carried out, to see if e.g. new species have formed which are beneficial for the Lebedev reaction, what the oxidation state of the metal species is (assumed to be in oxide states calculated with theoretical software) and what the exact deactivation behaviour is. Furthermore, other synthesis methods should be carried out to see if incipient wet impregnation is the correct technique for promotion of the wet-kneaded catalyst. Finally, changing the metal loading or alloying are the next steps in the promoter studies.

6 Concluding remarks and outlook

Butadiene is a useful bulk molecule in polymer industry. Due to the recent industrial feedstock shift towards shale gas, butadiene supply is limited. An attractive, sustainable alternative is the Lebedev process, where bioethanol is converted into butadiene. It is believed that ethanol is first dehydrogenated towards acetaldehyde. A subsequent aldol condensation and dehydration step yield crotonaldehyde, an α-β unsaturated aldehyde. Selective hydrogenation to crotyl alcohol is desired and a subsequent dehydration step yield butadiene. Previous work has shown that an overall well performing catalyst is a mixture of SiO_2 and MgO, where wet-kneading currently yields the most active catalyst. It is believed that magnesium silicates formed during wet-kneading are beneficial for ethanol conversion.
In this work, the wet-kneading parameters were optimised. Variations in wet-kneading volume and precursors have not influenced the catalyst significantly. Varying wet-kneading time allowed the formation of magnesium silicates to be followed. ^{1}H-^{29}Si CP-MAS NMR showed that the formed hydrous amorphous magnesium silicates correlate well to the unwanted ethylene production. Although it was believed that hydrous layered magnesium silicates are responsible for butadiene selectivity, no clear correlation was observed. An explanation could be the disappearance or blockage of other essential surface species due to the occurring cross deposition, such as MgO. Addition of NH_4NO_3 during wet-kneading yielded a highly selective catalyst towards ethylene, possibly due to the sole presence of hydrous amorphous magnesium silicates.
The addition of most promoters to the wet-kneaded catalyst led to an increased butadiene yield, with Cu and Ag showing the highest initial activity. However, most catalysts severely deactivated, presumably due to the increased formation of carbonacous compounds compared to the unpromoted catalyst. Mn promotion showed a moderate increase in butadiene yield with a high stability during reaction time. There are transition metals known from literature to increase butadiene selectivity, which have not yet been used as promoters in this research. These should be used for impregnation to complete the dataset. Finally, varying the metal loading, other metal loading techniques and alloying could lead to different catalytic behaviour.

Looking towards the future, the exact role of magnesium silicates during the Lebedev process remains unsolved. Therefore more studies need to be performed to give information about e.g. active sites, nature of both hydrous layered and amorphous magnesium silicates etc. As previously mentioned, magnesium silicates are known to contribute to the catalytic activity in the Lebedev process. Therefore testing pure or metal promoted magnesium silicates could yield an active catalyst in the Lebedev process. Furthermore, more characterisation of the impregnated catalyst needs to be carried out to give information about the topology of the promoters: have they been incorporated in the framework (e.g. formation of phyllosillicates), or are they present as nanoparticles? Also, the oxidation state has been determined by theoretical calculations, but need to be quantitatively confirmed. EXAFS and XANES measurements could amongst others clarify these questions. Catalyst regeneration has to be studied, before the catalyst could be used in upscaling experiments for eventual industrial applications. After 24 h on stream, the catalyst already suffers from carbonaceous deposition. To see whether deactivation is only caused by surface blockage due to carbonaceous deposition, recalcination

should first be carried out to see if the initial activity is maintained, or that the catalysts morphology has been changed during reaction conditions. Possible rehydration and calcination steps could restore the nature of magnesium silicates, should these be lost during reaction. However, impregnation with water as a control has shown to leave the magnesium silicate FT-IR band unaffected, meaning that the nature of magnesium silicates could still be the same. Finally, Angelici et *al.* stated that the addition of Cu not only improved the dehydrogenation properties of the catalyst, but also modified the acid-base properties.[28] Characterisation of the acid and basic sites still needs to be carried out for the all catalysts by e.g. $CHCl_3$-, CO- and pyridine adsorbed FT-IR spectroscopy, to determine the basic, Lewis acid and Brønsted sites, respectively. $CHCl_3$ adsorption gives a more reliable result than CO_2-TPD, due to the formation of carbonate species in CO_2-TPD which are harder to desorb.[28] However, quantification of adsorption IR spectroscopy for these catalysts is difficult. Since the hydroxyl vibrations are most likely consisting of different signals, there is no vibration signal present to normalise to. If possible, an external standard needs to be added for quantification.

References

[1] Angelici, C.; Weckhuysen, B.; Bruijnincx, P. *ChemSusChem* **2013**, *6*, 1595–614.

[2] OECD-FAO, Agricultural Outlook 2011-2020. 2012; http://stats.oecd.org/.

[3] Transparency Market Research, Synthetic And Bio-Based Butadiene Market: Industry Overview, Applications And Downstream Potential Opportunities, 2010 - 2018. http://www.transparencymarketresearch.com/synthetic-and-bio-based-butadiene-market.html.

[4] White, W. C. *Chem. Biol. Interact.* **2007**, *166*, 10–14.

[5] Mascal, M. *Biofuels, Bioprod. Biorefin.* **2012**, *6*, 483–493.

[6] Bruijnincx, P.; Weckhuysen, B. *Angew. Chem. Int. Ed.* **2013**, *52*, 11980–11987.

[7] Dow Chemical, *Product Safety Assessment: Butylenes*; 2012; 1-7.

[8] Arpe, H.-J. *Industrial Organic Chemistry*, 5th ed.; WILEY-VCH Verlag GmbH & Co. KGaA, 2010.

[9] Ipatiev, V. *J. prakt. Chem.* **1903**, *2*, 67–70.

[10] Ostromislenskiy, J. *J. Russ. Phys. Chem. Soc.* **1915**, *47*, 1472 –1506.

[11] Lebedev, S. *Russ. J. Gen. Chem.* **1933**, *3*, 698–708.

[12] Makshina, E.; Dusselier, M.; Janssens, W.; Degrève, J.; Jacobs, P.; Sels, B. *Chem. Soc. Rev.* **2014**, *43*, 7917–53.

[13] Patel, A. D.; Meesters, K.; den Uil, H.; de Jong, E.; Blok, K.; Patel, M. K. *Energy Environ. Sci.* **2012**, *5*, 8430.

[14] Posada, J. A.; Patel, A. D.; Roes, A.; Blok, K.; Faaij, A. P. C.; Patel, M. K. *Bioresour. Technol.* **2013**, *135*, 490–499.

[15] Cespi, D.; Passarini, F.; Vassura, I.; Cavani, F. *Green Chem.* **2015**, *00*, 1–45.

[16] Natta, G.; Rigamonti, R. *Chim. Ind.* **1947**, *29*, 195.

[17] Angelici, C.; Velthoen, M.; Weckhuysen, B.; Bruijnincx, P. *ChemSusChem* **2014**, *7*, 2505–2515.

[18] Janssens, W.; Makshina, E. V.; Vanelderen, P.; De Clippel, F.; Houthoofd, K.; Kerkhofs, S.; Martens, J. A.; Jacobs, P. A.; Sels, B. F. *ChemSusChem* **2015**, *8*, 994–1008.

[19] De Baerdemaeker, T.; Feyen, M.; Müller, U.; Yilmaz, B.; Xiao, F. S.; Zhang, W.; Yokoi, T.; Bao, X.; Gies, H.; De Vos, D. E. *ACS Catal.* **2015**, *5*, 3393–3397.

[20] Sushkevich, V. L.; Palagin, D.; Ivanova, I. I. *ACS Catal.* **2015**, *5*, 4833–4836.

[21] Bhattacharyya, S. K.; Ganguly, N. *J. appl. Chem* **1962**, *12*, 105–110.

[22] Bhattacharyya, S. K.; Ganguly, N. *J. appl. Chem* **1962**, *12*, 97–104.

[23] Chieregato, A.; Ochoa, J. V.; Bandinelli, C.; Fornasari, G.; Cavani, F.; Mella, M. *ChemSusChem* **2015**, *8*, 377–388.

[24] Gao, M.; Liu, Z.; Zhang, M.; Tong, L. *Catal. Lett.* **2014**, *144*, 2071–2079.

[25] Bhattacharyya, S. K.; Sanyal, S. *J. Catal.* **1967**, *7*, 152–158.

[26] Sushkevich, V. L.; Ivanova, I. I.; Ordomsky, V. V.; Taarning, E. *ChemSusChem* **2014**, *7*, 2527–36.

[27] Jones, M. D. *Chem. Cent. J.* **2014**, *8*, 53.

[28] Angelici, C.; Velthoen, M. E. Z.; Weckhuysen, B. M.; Bruijnincx, P. C. A. *Catal. Sci. Tech.* **2015**, *5*, 2869–2879.

[29] Aramend, A.; Borau, V.; Jiménez, C.; Marinas, J. M.; Ruiz, J. R.; Urbano, F. J. *Appl. Catal., A* **2003**, *244*, 207–215.

[30] Larina, O. V.; Kyriienko, P. I.; Soloviev, S. O. *Theor. Exp. Chem.* **2015**, *51*, 244–249.

[31] Zanella, R.; Louis, C.; Giorgio, S.; Touroude, R. *J. Catal.* **2004**, *223*, 328–339.

[32] Ponec, V. *Appl. Catal., A* **1997**, *149*, 27–48.

[33] Delbecq, F.; Sautet, P. *J. Catal.* **1995**, *152*, 217–236.

[34] Vannice, M. A.; Sen, B. *J. Catal.* **1989**, *115*, 65–78.

[35] Gallezot, P.; Richard, D. *Cat. Rev. - Sci. Eng.*; 1998; Vol. 40; pp 81–126.

[36] Baylon, R. A. L.; Sun, J.; Wang, Y. *Catal. Today* **2014**, *259*, 446–452.

[37] Sekiguchi, Y.; Akiyama, S.; Urakawa, W.; Koyama, T. R.; Miyaji, A.; Motokura, K.; Baba, T. *Catal. Commun.* **2015**, *68*, 20–24.

[38] Salman, F.; Park, C.; Baker, R. *Catal. Today* **1999**, *53*, 385–394.

[39] Reyes, P.; Rodr, C. *Catal. Lett.* **2000**, *69*, 27–32.

[40] Toebes, M.; Prinsloo, F.; Bitter, J.; Van Dillen, A.; De Jong, K. *J. Catal.* **2003**, *214*, 78–87.

[41] Raj, K.; Prakash, M. G.; Elangovan, T.; Viswanathan, B. *Catal. Lett.* **2011**, *142*, 87–94.

[42] Kvisle, S.; Aguero, A.; Sneeden, R. *Appl.Catal.* **1988**, *43*, 117–131.

[43] Chung, S.; Angelici, C.; Hinterding, S.; Weingarth, M.; Baldus, M.; Houben, K.; Weckhuysen, B.; Bruijnincx, P. A. *ACS Catal.* **2016**, *submitted*.

[44] Choi, I.; Smith, R. W. *J. Colloid Interface Sci.* **1972**, *40*, 253 – 262.

[45] Busey, R. H.; Mesmer, R. E. *Inorg. Chem.* **1977**, *16*, 2444–2450.

[46] RRUFF database. http://rruff.info/Antigorite, accessed on April 11, 2016.

[47] RRUFF database. http://rruff.info/Talc, accessed on April 11, 2016.

[48] Gruver, V.; Sun, A.; Fripiat, J. J. *Catal. Lett.* **1995**, *34*, 359–364.

[49] Makshina, E.; Janssens, W.; Sels, B.; Jacobs, P. *Catal. Today* **2012**, *198*, 338–344.

[50] Vatsha, B.; Tetyana, P.; Shumbula, P. M.; Ngila, J. C.; Sikhwivhilu, L. M.; Moutloali, R. M. *J. Biomater. Nanobiotechnol.* **2013**, *4*, 365–373.

[51] Ochoa, J. V.; Bandinelli, C.; Vozniuk, O.; Chieregato, A.; Malmusi, A.; Recchi, C.; Cavani, F. *Green Chem.* **2015**, *00*, 1–11.

[52] Ohnishi, R.; Akimoto, T.; Tanabe, K. *J. Chem. Soc., Chem. Commun.* **1985**, *70*, 1613.

[53] Zhang, M.; Gao, M.; Chen, J.; Yu, Y. *RSC Adv.* **2015**, *5*, 25959–25966.

[54] Lewandowski, M.; Babu, G. S.; Vezzoli, M.; Jones, M. D.; Owen, R. E.; Mattia, D.; Plucinski, P.; Mikolajska, E.; Ochenduszko, A.; Apperley, D. C. *Catal. Commun.* **2014**, *49*, 25–28.

[55] Larina, O. V.; Kyriienko, P. I.; Soloviev, S. O. *Catal. Lett.* **2015**, *145*, 1162–1168.

[56] Evonik Industries AG, *Technical Bulletin Fine Particles No. 27, AEROSIL fumed silica for solvent-free epoxy resins*; 1-19, accessed on May 5, 2016.

[57] Giorgi, R.; Bozzi, C.; Dei, L.; Gabbiani, C.; Ninham, B. W.; Baglioni, P. *Langmuir* **2005**, *21*, 8495–8501.

[58] Ding, Y.; Zhang, G.; Wu, H.; Hai, B.; Wang, L.; Qian, Y. *Chem. Mater.* **2001**, *13*, 435–440.

[59] Makhluf, S.; Dror, R.; Nitzan, Y.; Abramovich, Y.; Jelinek, R.; Gedanken, A. *Adv. Funct. Mater.* **2005**, *15*, 1708–1715.

[60] Maliyekkal, S. M.; Anshup,; Antony, K. R.; Pradeep, T. *Sci. Total Environ.* **2010**, *408*, 2273–82.

[61] Luhmer, M.; d'Espinose, J.; Hommel, H.; Legrand, A. *Magn. Reson. Imaging* **1996**, *14*, 911 – 913.

[62] McCarty, R. J.; Palke, A. C.; Stebbins, J. F.; Hartman, S. *Am. Mineral.* **2015**, *100*, 1265–1276.

[63] Stebbins, J. F.; Panero, W. R.; Smyth, J. R.; Frost, D. J. *Am. Mineral.* **2009**, *94*, 626–629.

[64] de la Caillerie, E.; Kermarec, M.; Clause, O. *J. Phys. Chem* **1995**, *99*, 17273–17281.

[65] Walling, S. A.; Kinoshita, H.; Bernal, S. A.; Collier, N. C.; Provis, J. L. *Dalton Trans.* **2015**, *44*, 8126–8137.

[66] Chabrol, K.; Gressier, M.; Pebere, N.; Menu, M.-J.; Martin, F.; Bonino, J.-P.; Marichal, C.; Brendle, J. *J. Mater. Chem.* **2010**, *20*, 9695–9706.

[67] MacKenzie, K. J. D.; Bradley, S.; Hanna, J. V.; Smith, M. E. *J. Mater. Sci.* **2013**, *48*, 1787–1793.

[68] Fellner, P.; Híveš, J.; Khandl, V.; Králik, M.; Jurišová, J. *Chem. Pap.* **2011**, *65*, 454–459.

[69] Sing, K. *Colloids Surf., A* **2001**, *187188*, 3 – 9.

[70] Richter, M.; Bentrup, U.; Eckelt, R.; Schneider, M.; Pohl, M.-M.; Fricke, R. *Appl. Catal., B* **2004**, *51*, 261 – 274.

[71] Angelici, C.; Meirer, F.; Van Der Eerden, A. M. J.; Schaink, H. L.; Goryachev, A.; Hofmann, J. P.; Hensen, E. J. M.; Weckhuysen, B. M.; Bruijnincx, P. C. A. *ACS Catal.* **2015**, *5*, 6005–6015.

[72] RRUFF database. http://rruff.info/Grunerite, accessed on April 11, 2016.

[73] Majewski, A. J.; Wood, J.; Bujalski, W. *Int. J. Hydrogen Energy* **2013**, *38*, 14531 – 14541.

[74] Kitayama, Y.; Michishita, A. *J. Chem. Soc., Chem. Commun.* **1981**, 401–402.

[75] Kitayama, Y.; Satoh, M.; Kodama, T. *Catal. Lett.* **1996**, *36*, 95–97.

[76] Bachiller-Baeza, B.; Rodríguez-Ramos, I.; Guerrero-Ruiz, A. *Appl. Catal., Al* **2001**, *205*, 227–237.

[77] Kawabata, T.; Matsuoka, H.; Shishido, T.; Li, D.; Tian, Y.; Sano, T.; Takehira, K. *Appl. Catal. A* **2006**, *308*, 82 – 90.

[78] Ezinkwo, G. O.; Tretyakov, V. P.; Aliyu, A.; Ilolov, A. M. *ChemBioEng Rev.* **2014**, *1*, 194–203.

[79] North, M., Ed. *Sustainable Catalysis with Non-endangered Metals, Parts 1 and 2*; RSC Green Chemistry; The Royal Society of Chemistry, 2016; 318 - 324.

[80] Chorkendorff, I.; Niemantsverdriet, J. W. *Concepts of Modern Catalysis and Kinetics*; Wiley-VCH Verlag GmbH & Co. KGaA, 2005; 301–348.

[81] Han, Z.; Li, X.; Zhang, M.; Liu, Z.; Gao, M. *RSC Adv.* **2015**, 103982–103988.

[82] Corson, B.; Jones, H.; Welling, C.; Hinckley, J.; Stahly, E. *Ind. Eng. Chem.* **1950**, *42*, 359–373.

[83] Toussaint, W. J.; Dunn, J. T.; Jachson, D. R. *Ind. Eng. Chem.* **1947**, *39*, 120–125.

[84] Quattlebaum, W. M.; Toussaint, W. J.; Dunn, J. T. *J. Am. Chem. Soc.* **1947**, *69*, 593–599.

[85] Gnep, N.; Doyement, J.; Guisnet, M. *J. Mol. Catal.* **1988**, *45*, 281–284.

[86] Guisnet, M.; Gnep, N.; Alario, F. *Appl. Catal. A* **1992**, *89*, 1–30.

[87] Concepción, P.; Corma, A.; Silvestre-Albero, J.; Franco, V.; Chane-Ching, J. Y. *J. Am. Chem. Soc.* **2004**, *126*, 5523–5532.

[88] Jones, M.; Keir, C.; Iulio, C.; Robertson, R.; Williams, C.; Apperley, D. *Catal. Sci. Tech.* **2011**, *1*, 267.

[89] Sushkevich, V. L.; Ivanova, I. I.; Taarning, E. *Green Chem.* **2015**, *17*, 2552–2559.

[90] Borgna, A.; Borgna, A.; Anderson, B. G.; Anderson, B. G.; Saib, A. M.; Saib, A. M.; Bluhm, H.; Bluhm, H.; Ha, M.; Ha, M.; Knop-gericke, A.; Knop-gericke, A.; Tamminga, Y.; Tamminga, Y. *J. Phys. Chem. B* **2004**, *108*, 17905–17914.

[91] Tsang, S. C.; Cailuo, N.; Oduro, W.; Kong, A. T. S.; Clifton, L.; Yu, K. M. K.; Thiebaut, B.; Cookson, J.; Bishop, P. *ACS Nano* **2008**, *2*, 2547–2553.

Acknowledgements

Writing my Master thesis was an emotional rollercoaster. Successes followed by set-backs are often encountered, long nights to finish deadlines, broken set-ups, and all combined with rowing eight times a week: it has been one hell of a ride. But what a ride it has been, and looking back: a quite short ride; it is over before you know it. During my Master programme I have become well acquainted with research, a wonderful experience. And I would not have learned this much without the wonderful people that helped me throughout the year.
First of all, I would like to sincerely thank Dr. Sang-Ho Chung and Dr. Pieter Bruijnincx for teaching and supervision, helping me with my work, brainstorming, revising presentations and the NCCC poster, but most of all this final work. I have learned so much from you, many thanks for all your input and invested time. I wish you the best of luck with your careers and a happy, prosperous life. Dr. Carlo Angelici is thanked for the assistance when Sang-Ho was unavailable. Prof. Petra de Jongh, thank you for being my second reader for my thesis. Prof. Bert Weckhuysen, thank you for the possibility to work in your group for a year.
Lennart Weber and prof. Krijn de Jong, thank you for supervision for my literature study. Although I was struggling a while on the subject and the layout for the document, I am more than pleased with the result. Again, I have learned a lot from the study and has helped developing my writing skills.
Prof. Marc Baldus and Dr. Klaartje Houben are greatly acknowledged for the amount of work invested in NMR analysis and assistance for measurements.
Wouter Lamme, Lisette Pompe and Katinka Wondergem are acknowledged for TEM measurements. Peter Bramwell and Suzanne Verkleij are thanked for nitrogen physisorbtion measurements. Ramon Oord, many thanks for the fast NH_3-TPD measurements. Fouad Soulimani, thank you for helping me with the FT-IR set-up. Ing. Helen de Waard from the Utrecht University GeoLab is thanked for ICP-OES measurements.
I would like to thank Ad Mens, Ad van der Eerden and Pascal Wijten for supplying me with parts for the reactor, technical assistance and help during malfunctions. Your help when the setup was malfunctioning was needed a lot.
Finally, a sincere thanks for the entire Inorganic Chemistry & Catalysis group for the great borrels, labuitje and friendly work environment. It is a great place to work.

Appendices

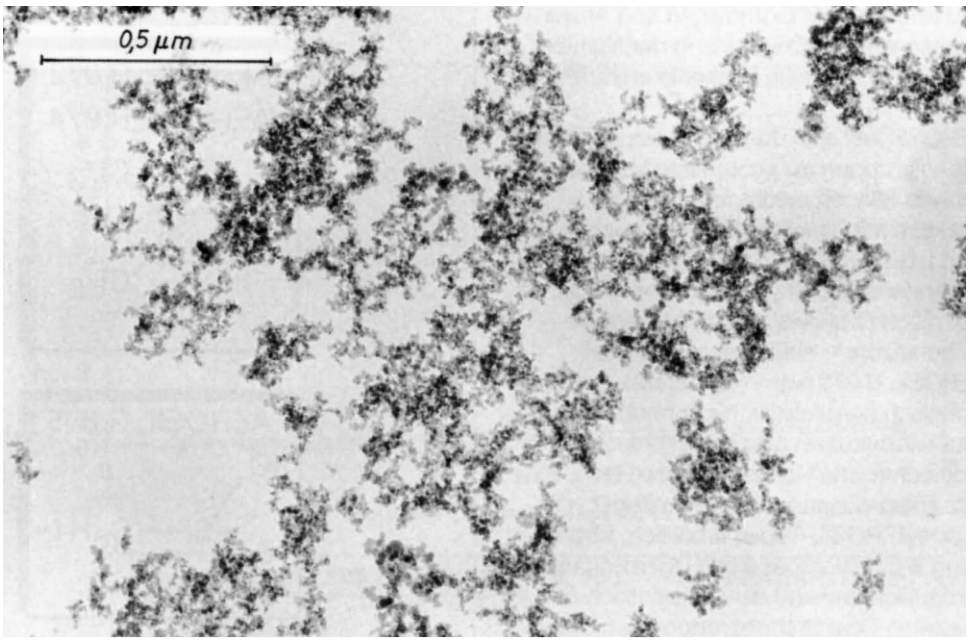

Appendix 1. *TEM image of Aerosil-300, courtesy of Evonik.*[56]

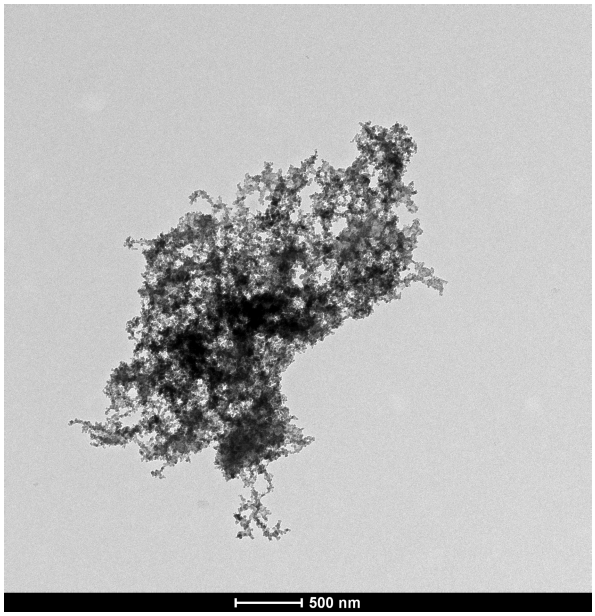

Appendix 2. *TEM image of Aerosil-380.*

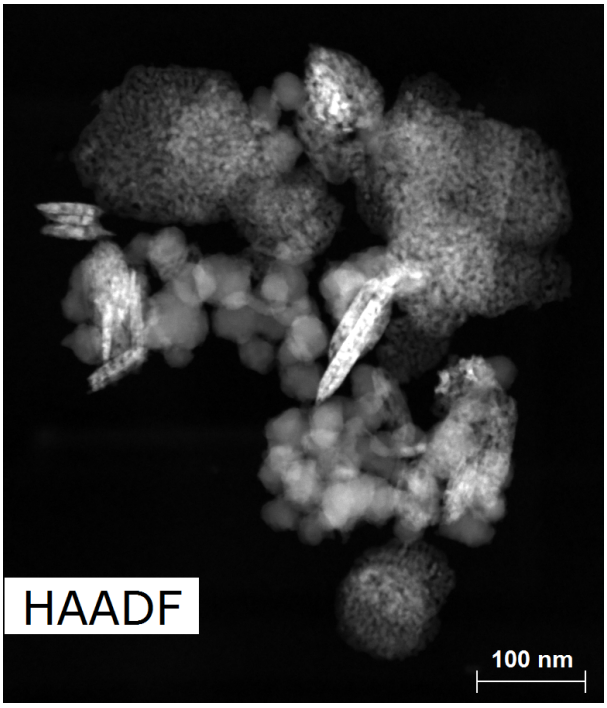

Appendix 3. *HAADF TEM image of the SiO_2-nMgO catalyst, wet-kneaded for 0.5 h.*

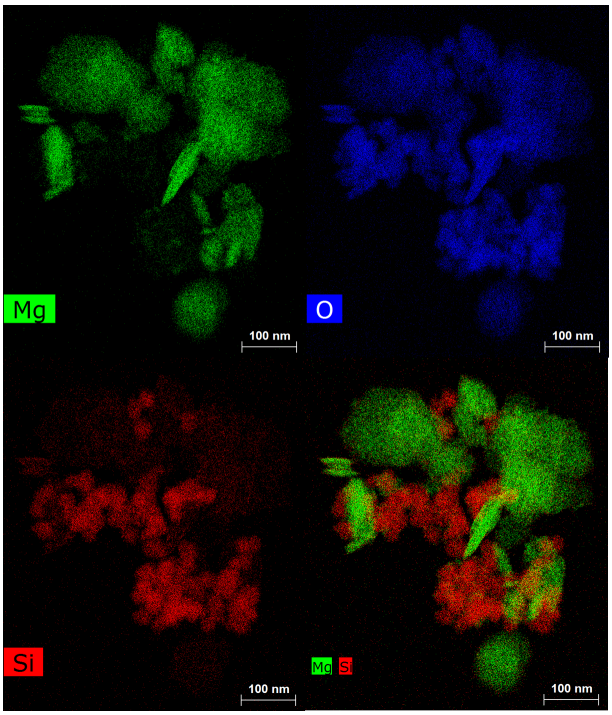

Appendix 4. *TEM-EDX map of the SiO_2-nMgO catalyst, wet-kneaded for 0.5 h.*

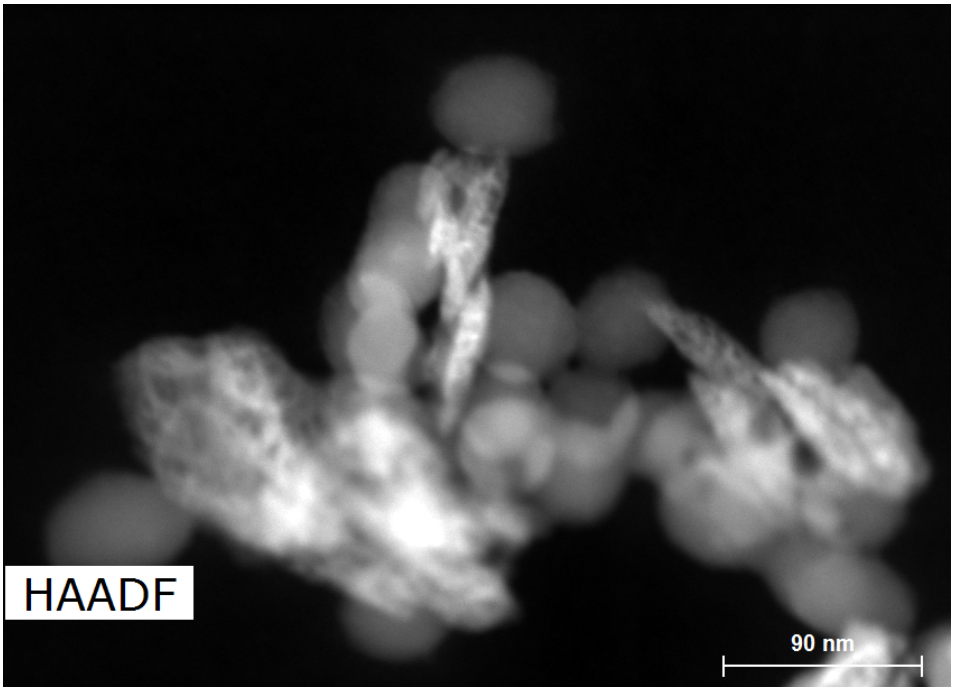

Appendix 5. *HAADF TEM image of the SiO_2-nMgO catalyst, wet-kneaded for 4 h.*

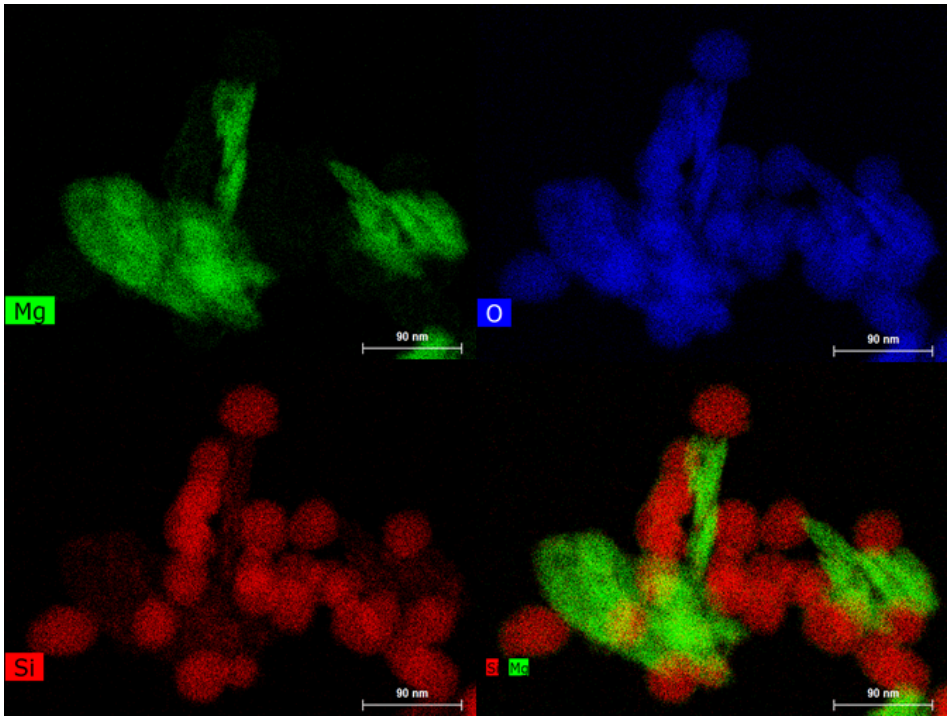

Appendix 6. *TEM-EDX map of the SiO_2-nMgO catalyst, wet-kneaded for 4 h.*

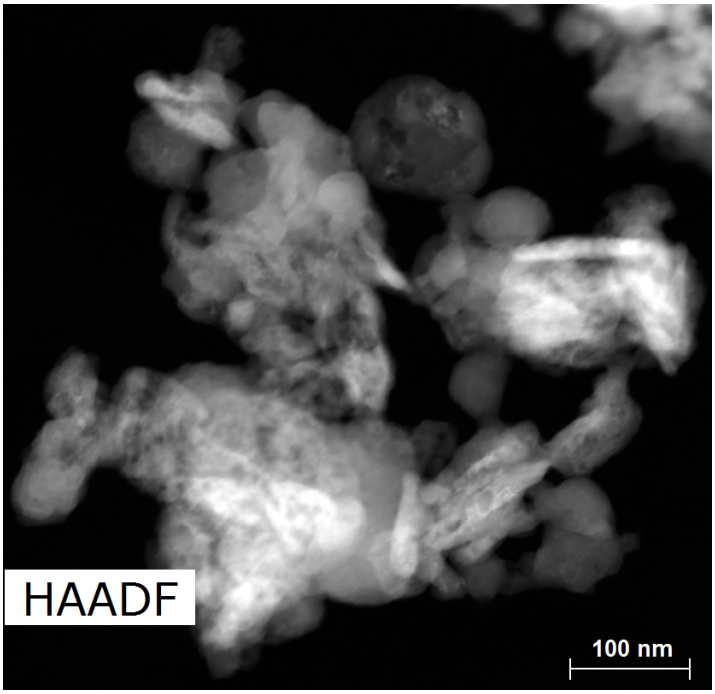

Appendix 7. *HAADF TEM image of the SiO_2-nMgO catalyst, wet-kneaded for 168 h.*

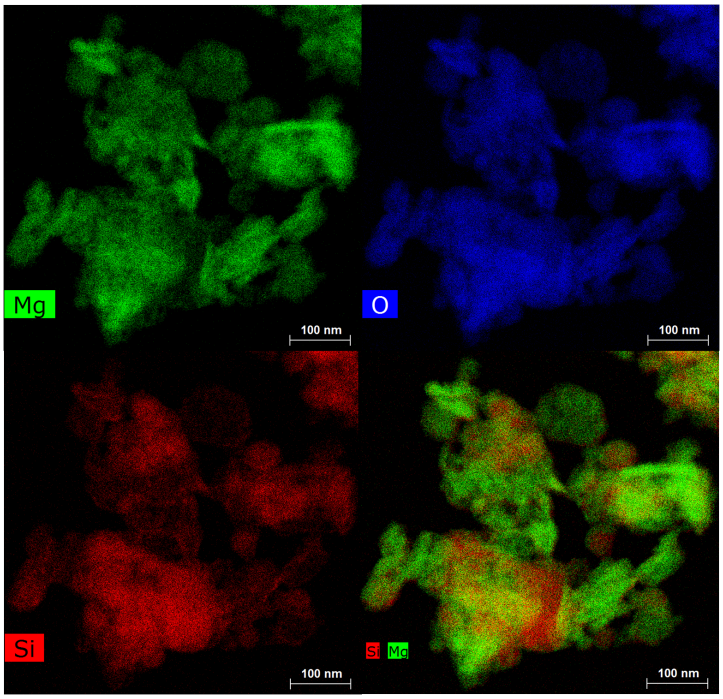

Appendix 8. *TEM-EDX map of the SiO_2-nMgO catalyst, wet-kneaded for 168 h.*

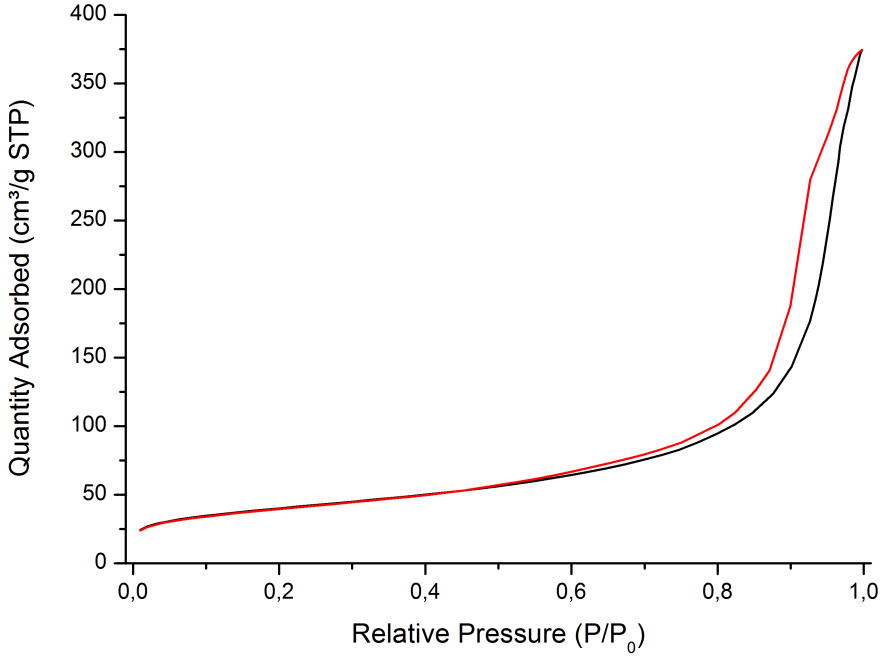

Appendix 9. *N_2-physisorption data of the SiO_2-nMgO catalyst, 4 h wet-kneading time, with the adsorption isotherm in black and the desorption isotherm in red.*

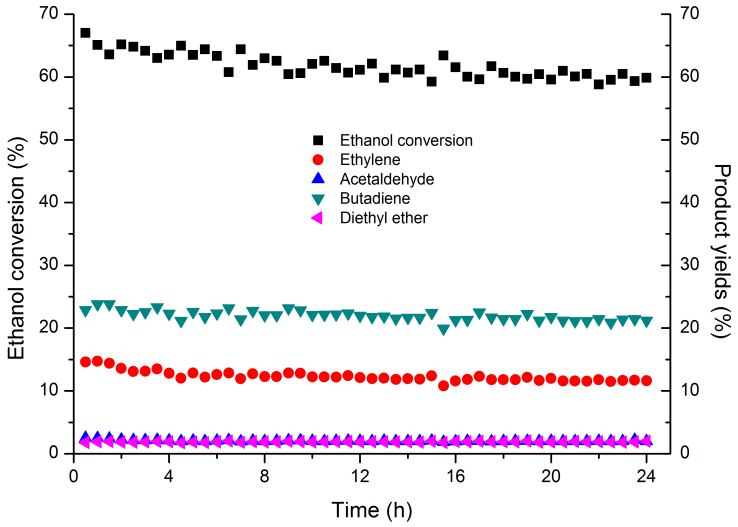

Appendix 10. *Catalytic data of the unpromoted wet-kneaded SiO_2-nMgO catalyst.*

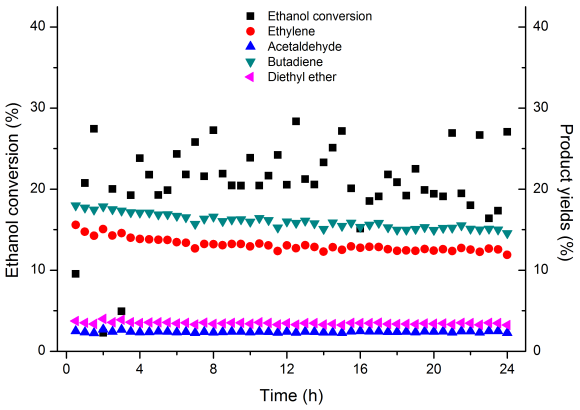

Appendix 11. *Catalytic data of the Zr impregnated wet-kneaded SiO_2-nMgO catalyst.*

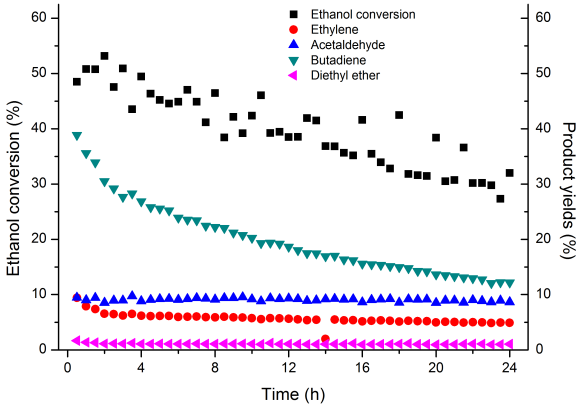

Appendix 12. *Catalytic data of the Mo impregnated wet-kneaded SiO_2-nMgO catalyst.*

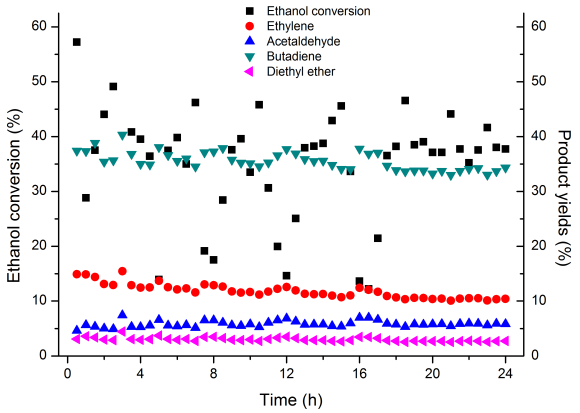

Appendix 13. *Catalytic data of the Mn impregnated wet-kneaded SiO_2-nMgO catalyst.*

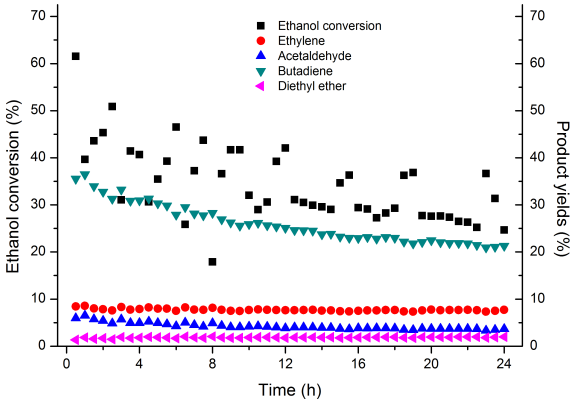

Appendix 14. *Catalytic data of the Fe impregnated wet-kneaded SiO_2-nMgO catalyst.*

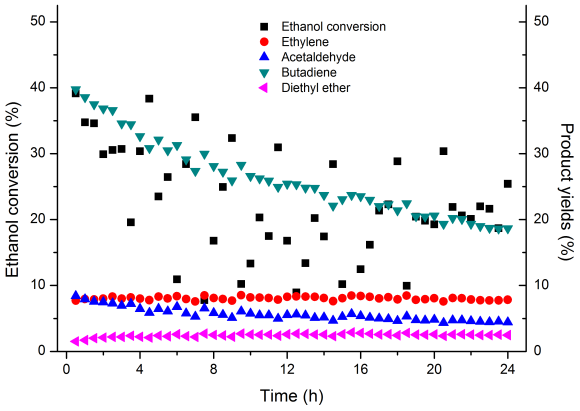

Appendix 15. *Catalytic data of the Ru impregnated wet-kneaded SiO_2-nMgO catalyst.*

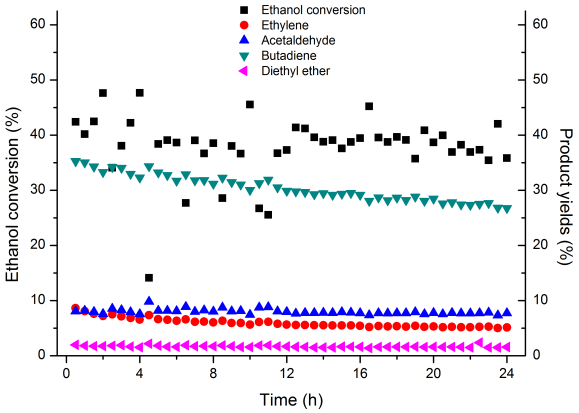

Appendix 16. *Catalytic data of the Co impregnated wet-kneaded SiO_2-nMgO catalyst.*

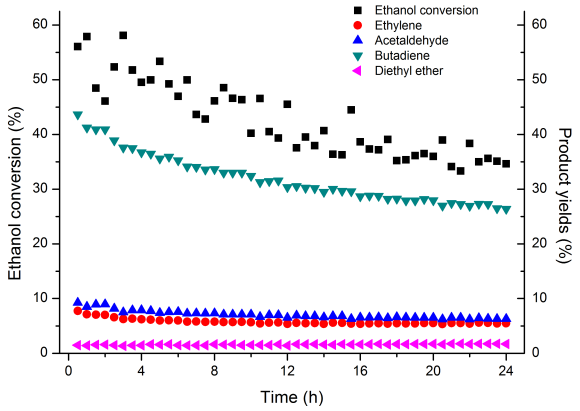

Appendix 17. *Catalytic data of the Ni impregnated wet-kneaded SiO_2-nMgO catalyst.*

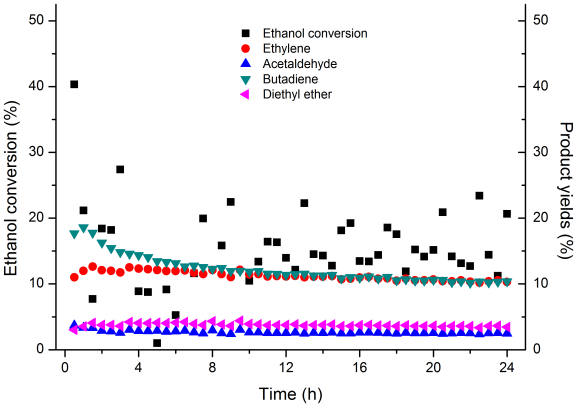

Appendix 18. *Catalytic data of the Pd impregnated wet-kneaded SiO_2-nMgO catalyst.*

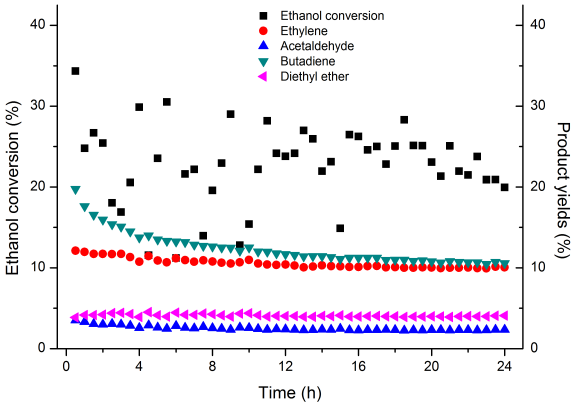

Appendix 19. *Catalytic data of the Pt impregnated wet-kneaded SiO_2-nMgO catalyst.*

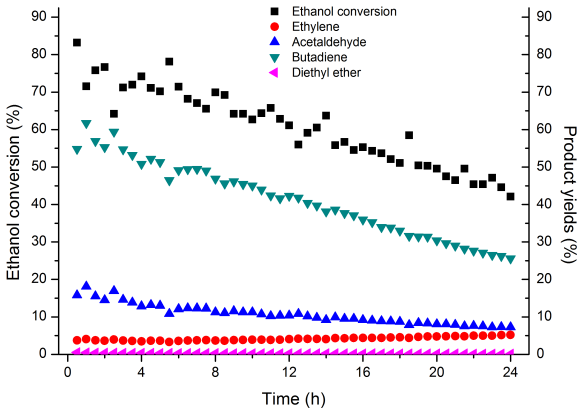

Appendix 20. *Catalytic data of the Cu impregnated wet-kneaded SiO_2-nMgO catalyst.*

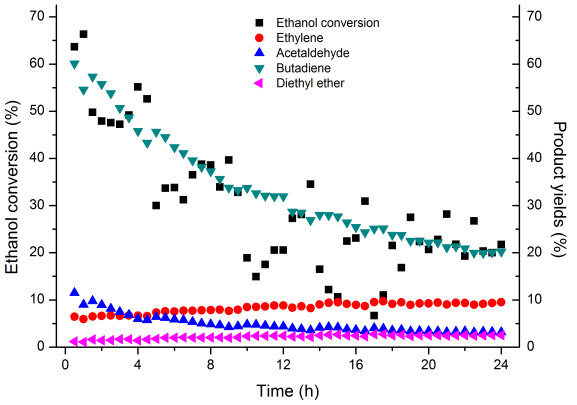

Appendix 21. *Catalytic data of the Ag impregnated wet-kneaded SiO_2-nMgO catalyst.*

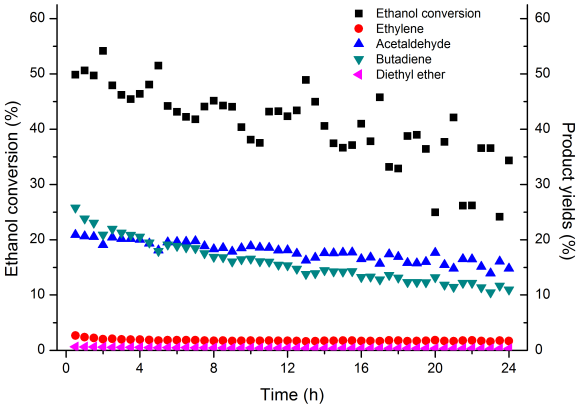

Appendix 22. *Catalytic data of the Zn impregnated wet-kneaded SiO_2-nMgO catalyst.*

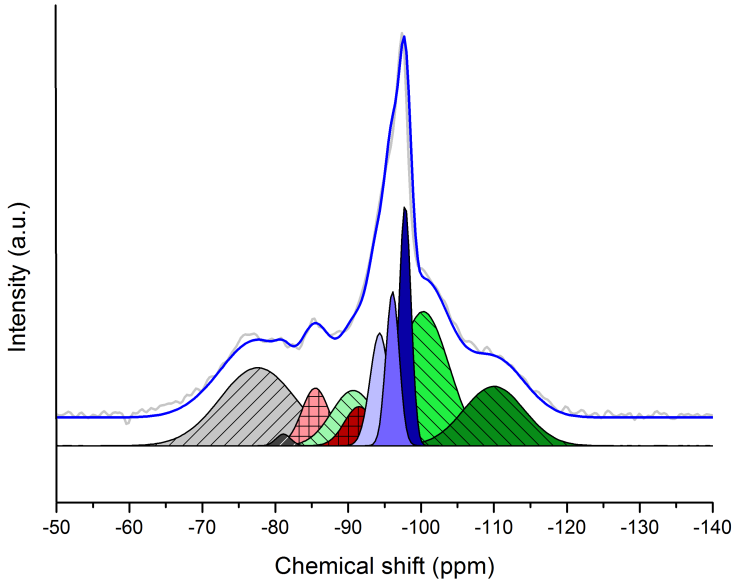

Appendix 23. *^{1}H-^{29}Si CP-MAS NMR spectrum and deconvoluted signals of the SiO_2-nMgO catalyst, wet-kneaded for 0.5 h.*

Table 5. *NMR peak data of the SiO_2-nMgO catalyst, wet-kneaded for 0.5 h. The retrieved peak area has been divided by the number of scans (33536) to yield the peak absolute area.*

Chemical shift (ppm)	FWHM	Peak absolute area (a.u.)	Area %
-77.6	6.10	7294.2	20.6
-81.1	1.17	234.9	0.7
-85.5	2.20	1939.6	5.5
-91.5	2.35	1267.4	3.6
-94.3	2.63	2758.4	7.8
-96.1	1.06	2143.8	6.0
-97.8	0.95	3537.7	10.0
-90.7	3.51	3236.7	9.1
-100.3	4.11	8754.0	24.7
-110.0	4.87	4311.5	12.2

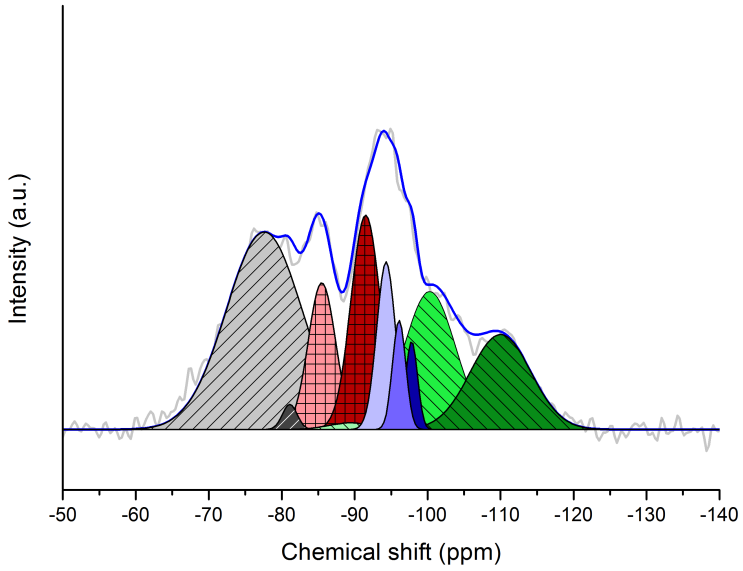

Appendix 24. *^{1}H-^{29}Si CP-MAS NMR spectrum and deconvoluted signals of the SiO_2-nMgO catalyst, wet-kneaded for 2 h.*

Table 6. *NMR peak data of the SiO_2-nMgO catalyst, wet-kneaded for 2 h. The retrieved peak area has been divided by the number of scans (22528) to yield the peak absolute area.*

Chemical shift (ppm)	FWHM	Peak absolute area (a.u.)	Area %
-77.6	6.10	6484.8	33.8
-81.1	1.17	152.1	0.8
-85.5	2.20	1742.5	9.1
-91.5	2.35	2520.8	13.1
-94.3	2.63	1439.1	7.5
-96.1	1.06	551.1	2.9
-97.8	0.95	458.0	2.4
-90.7	3.51	301.8	1.6
-100.3	4.11	3057.2	15.9
-110.0	4.87	2480.5	12.9

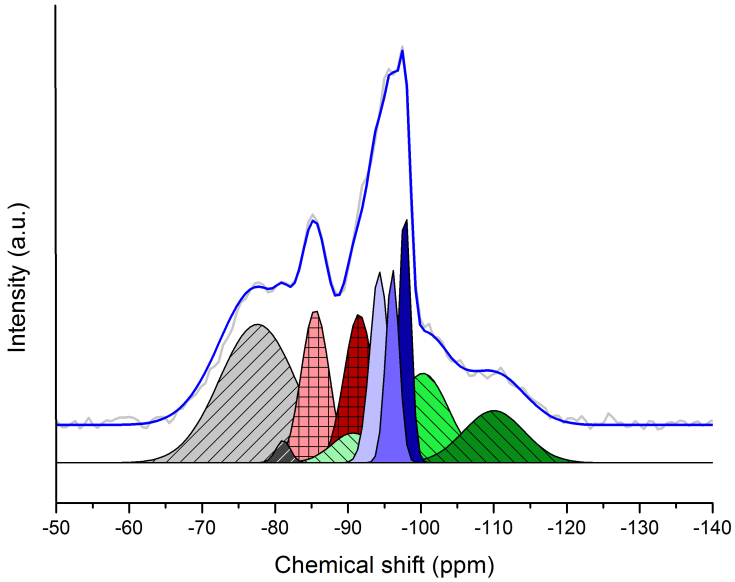

Appendix 25. *^{1}H-^{29}Si CP-MAS NMR spectrum and deconvoluted signals of the SiO_2-nMgO catalyst, wet-kneaded for 4 h.*

Table 7. *NMR peak data of the SiO_2-nMgO catalyst, wet-kneaded for 4 h. The retrieved peak area has been divided by the number of scans (67584) to yield the peak absolute area.*

Chemical shift (ppm)	FWHM	Peak absolute area (a.u.)	Area %
-77.6	6.10	5485.4	27.7
-81.1	1.17	163.9	0.8
-85.5	2.20	2323.0	11.7
-91.5	2.35	2413.1	12.2
-94.3	2.63	1888.6	9.5
-96.1	1.06	1357.7	6.9
-97.8	0.95	1523.9	7.7
-90.7	3.51	516.9	2.6
-100.3	4.11	2553.0	12.9
-110.0	4.87	1552.6	7.8

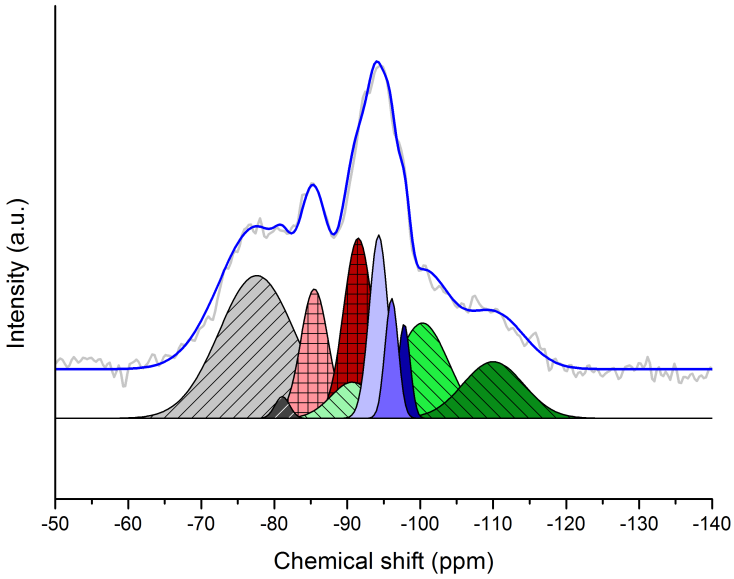

Appendix 26. *^{1}H-^{29}Si CP-MAS NMR spectrum and deconvoluted signals of the SiO_2-nMgO catalyst, wet-kneaded for 24 h.*

Table 8. *NMR peak data of the SiO_2-nMgO catalyst, wet-kneaded for 24 h. The retrieved peak area has been divided by the number of scans (22528) to yield the peak absolute area.*

Chemical shift (ppm)	FWHM	Peak absolute area (a.u.)	Area %
-77.6	6.10	6357.0	29.6
-81.1	1.17	223.4	1.0
-85.5	2.20	2247.7	10.5
-91.5	2.35	3128.7	14.6
-94.3	2.63	2098.4	9.8
-96.1	1.06	976.3	4.5
-97.8	0.95	746.8	3.5
-90.7	3.51	867.1	4.0
-100.3	4.11	2849.1	13.3
-110.0	4.87	2001.2	9.3

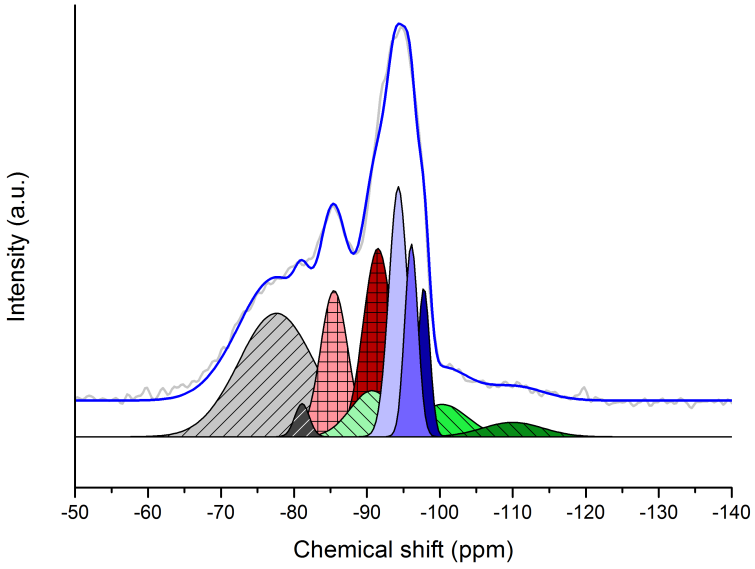

Appendix 27. *^{1}H-^{29}Si CP-MAS NMR spectrum and deconvoluted signals of the SiO_2-nMgO catalyst, wet-kneaded for 48 h.*

Table 9. *NMR peak data of the SiO_2-nMgO catalyst, wet-kneaded for 48 h. The retrieved peak area has been divided by the number of scans (22528) to yield the peak absolute area.*

Chemical shift (ppm)	FWHM	Peak absolute area (a.u.)	Area %
-77.6	6.10	9664.1	28.6
-81.1	1.17	471.7	1.4
-85.5	2.20	4003.3	11.8
-91.5	2.35	5654.5	16.7
-94.3	2.63	4720.7	14.0
-96.1	1.06	2638.5	7.8
-97.8	0.95	1735.9	5.1
-90.7	3.51	2149.2	6.4
-100.3	4.11	1835.6	5.4
-110.0	4.87	930.4	2.8

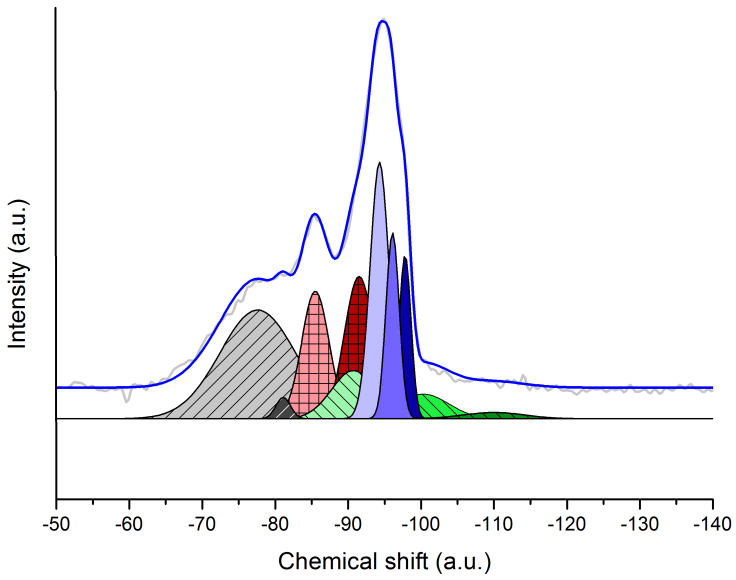

Appendix 28. *^{1}H-^{29}Si CP-MAS NMR spectrum and deconvoluted signals of the SiO_2-nMgO catalyst, wet-kneaded for 168 h.*

Table 10. *NMR peak data of the SiO_2-nMgO catalyst, wet-kneaded for 168 h. The retrieved peak area has been divided by the number of scans (22528) to yield the peak absolute area.*

Chemical shift (ppm)	FWHM	Peak absolute area (a.u.)	Area %
-77.6	6.10	10522.0	27.6
-81.1	1.17	401.9	1.1
-85.5	2.20	4750.4	12.5
-91.5	2.35	6091.5	16.0
-94.3	2.63	6184.3	16.2
-96.1	1.06	3362.5	8.8
-97.8	0.95	2479.6	6.5
-90.7	3.51	2135.6	5.6
-100.3	4.11	1569.9	4.1
-110.0	4.87	578.7	1.5